



**UNIVERSIDADE FEDERAL DE UBERLÂNDIA  
FACULDADE DE ENGENHARIA QUÍMICA  
PROGRAMA DE PÓS-GRADUAÇÃO EM  
ENGENHARIA QUÍMICA**



**HYDROGEN PRODUCTION FROM THE STEAM REFORMING OF  
LIQUEFIED PETROLEUM GAS USING NICKEL BASED PRECURSORS.**

*PRODUÇÃO DE HIDROGÊNIO A PARTIR DA REFORMA A VAPOR DO GÁS  
LIQUEFEITO DE PETRÓLEO USANDO PRECURSORES A BASE DE NÍQUEL.*

**RAFAEL PACHECO BORGES**

**UBERLÂNDIA – MG**

2019



**UNIVERSIDADE FEDERAL DE UBERLÂNDIA**  
**FACULDADE DE ENGENHARIA QUÍMICA**  
**PROGRAMA DE PÓS-GRADUAÇÃO EM**  
**ENGENHARIA QUÍMICA**



**HYDROGEN PRODUCTION FROM THE STEAM REFORMING OF  
LIQUEFIED PETROLEUM GAS USING NICKEL BASED PRECURSORS.**

*PRODUÇÃO DE HIDROGÊNIO A PARTIR DA REFORMA A VAPOR DO GÁS  
LIQUEFEITO DE PETRÓLEO USANDO PRECURSORES A BASE DE NÍQUEL.*

Rafael Pacheco Borges

Orientadora: Dr<sup>a</sup> Carla Eponina Hori

Coorientador: Dr. Fábio Bellot Noronha

Tese submetida ao Programa de Pós-Graduação em Engenharia Química da Universidade Federal de Uberlândia como parte dos requisitos necessários à obtenção do título de Doutor em Engenharia Química.

Dados Internacionais de Catalogação na Publicação (CIP)  
Sistema de Bibliotecas da UFU, MG, Brasil.

---

B732h  
2019      Borges, Rafael Pacheco, 1988-  
            Hydrogen production from the steam reforming of liquefied  
            petroleum gas using nickel based precursors [recurso eletrônico] =  
            Produção de hidrogênio a partir da reforma a vapor do gás liquefeito de  
            petróleo usando precursores a base de níquel / Rafael Pacheco Borges. -  
            2019.

Orientadora: Carla Eponina Hori.

Coorientador: Fábio Bellot Noronha.

Tese (Doutorado) - Universidade Federal de Uberlândia, Programa  
de Pós-Graduação em Engenharia Química.

Disponível em: <http://doi.org/10.14393/ufu.te.2020.3018>

Inclui bibliografia.

Inclui ilustrações.

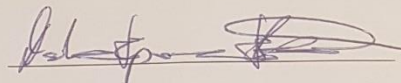
I. Engenharia química. I. Hori, Carla Eponina, 1965-, (Orient.). II.  
Noronha, Fábio Bellot, 1963-, (Coorient.). III. Universidade Federal de  
Uberlândia. Programa de Pós-Graduação em Engenharia Química. IV.  
Título.

---

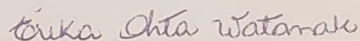
CDU: 66.0

TESE DE DOUTORADO SUBMETIDA AO PROGRAMA DE PÓS-GRADUAÇÃO EM ENGENHARIA QUÍMICA DA UNIVERSIDADE FEDERAL DE UBERLÂNDIA COMO PARTE DOS REQUISITOS NECESSÁRIOS PARA OBTENÇÃO DO TÍTULO DE DOUTOR EM ENGENHARIA QUÍMICA, EM 20 DE SETEMBRO DE 2019.

BANCA EXAMINADORA



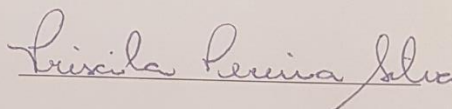
Prof<sup>a</sup>.Dr<sup>a</sup> Carla Eponina Hori  
Orientadora (PPGEQ/UFU)



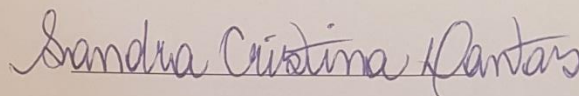
Prof<sup>a</sup>.Dr<sup>a</sup>Érika Otha Watanabe  
(FEQ/UFU)



Prof<sup>a</sup>.Dr<sup>a</sup>. Lucienne Lobato Romanielo  
(FEQ/UFU)



Prof<sup>a</sup>.Dr<sup>a</sup>Priscila Pereira Silva  
(Engenharia Química/ICTE-UFTM)



Prof<sup>a</sup>.Dr<sup>a</sup>Sandra Cristina Dantas  
(Engenharia Química/ICTE-UFTM)

## SUMMARY

FIGURE LIST .....	iii
TABLE LIST .....	v
ABSTRACT.....	vi
RESUMO.....	vii
1. INTRODUCTION .....	1
2. LITERATURE REVIEW .....	4
3. HYDROGEN PRODUCTION FROM THE STEAM REFORMING OF LPG USING SUPPORTED PEROVSKITES PRECURSORS .....	12
3.1. Introduction .....	13
3.2. Methodology .....	16
3.3. Results and Discussion.....	19
3.3.1. Catalysts Characterization .....	19
3.3.2. Stability Tests – Steam Reforming of LPG.....	25
3.3.3. Thermogravimetric Analysis (TGA) .....	31
3.4. Conclusions .....	32
4. HYDROGEN PRODUCTION FROM THE STEAM REFORMING OF PROPANE USING CERIA-SILICA SUPPORTED NICKEL PRECURSORS .....	34
4.1. Introduction .....	35
4.2. Methodology .....	38
4.3. Results and Discussion.....	42
4.3.1. Catalysts Characterization .....	42
4.3.2. Stability Tests – Steam Reforming of LPG.....	50
4.3.3. Thermogravimetric Analysis (TGA) .....	53
4.4. Conclusions .....	54
REFERENCES .....	55

## FIGURE LIST

<b>Figure 1.1.</b> Energy production sources in the USA (2003) .....	1
<b>Figure 2.1.</b> Moles of hydrogen produced per mol of reacted propane, as a function of temperature and WPR at atmospheric pressure. ....	5
<b>Figure 2.2.</b> Theoretical scheme of a perovskite structure .....	8
<b>Figure 2.3.</b> (A) LPG conversion of perovskite-derived catalysts at 873 K (B) LPG conversion at different temperatures using $\text{La}_{0.95}\text{Ce}_{0.05}\text{NiO}_3$ catalyst during the steam reforming process. Feed Condition: LPG/H <sub>2</sub> O = 1/7; W/F = 0.05 mg*min/L. ....	9
<b>Figure 2.4.</b> Methane and CO <sub>2</sub> conversion versus TOS for DRM at 1073 K and CH <sub>4</sub> /CO <sub>2</sub> = 1.0 over (a) LaNiO <sub>3</sub> ; (b) LaNiO <sub>3</sub> /Al <sub>2</sub> O <sub>3</sub> ; (c) LaNiO <sub>3</sub> /CeSiO <sub>2</sub> (Rabelo-Neto et al., 2018) .....	10
<b>Figure 3.1.</b> <i>in situ</i> XRD diffractograms of perovskite derived precursors: (A) LaNi; (B) LaNi/CS; (C) LaNi/AL .....	21
<b>Figure 3.2.</b> XANES spectra at the Ni K-edge during the reduction under 5%H <sub>2</sub> /He mixture of the perovskite-derived precursors: (A) LaNi; (B) LaNi/CS; (C) LaNi/AL.....	23
<b>Figure 3.3.</b> XANES treatment during the reduction of perovskite derived precursor LaNi/CS.....	24
<b>Figure 3.4.</b> LPG conversion during the SRLPG at 600 °C over the perovskite-derived catalysts .....	25
<b>Figure 3.5.</b> Species molar fraction during the SRLPG at 600 °C over the perovskite-derived catalysts. (A) LaNi; (B) LaNi/CS; and (C) LaNi/AL .....	26
<b>Figure 3.6.</b> LPG conversion during the SRLPG at 700 °C over the perovskite-derived catalysts .....	29
<b>Figure 3.7.</b> Species molar fraction during the SRLPG at 700°C over the perovskite-derived catalysts LaNi (A), LaNi/CS (B) and LaNi/AL (C) .....	30
<b>Figure 4.1.</b> <i>in situ</i> XRD diffractograms of supported nickel precursors Ni/65CS (A), Ni/75CS (B), Ni/85CS (C) and NiCe (D).....	43
<b>Figure 4.2.</b> TPR profile of the ceria-silica supported Ni precursors.....	45

<b>Figure 4.3.</b> <i>In situ</i> XANES performed in Ni K-edge during the reduction process of supported nickel precursors Ni/65CS (A), Ni/75CS (B), Ni/85CS (C) and NiCe (D) .....	46
<b>Figure 4.4.</b> <i>In situ</i> XANES performed in Ni K edge during the SRP reaction using the supported nickel catalyst Ni/65CS (A).....	47
<b>Figure 4.5.</b> <i>In situ</i> XANES performed in Ce L <sub>III</sub> edge during the reduction process of supported nickel precursors Ni/65CS (A), Ni/75CS (B), Ni/85CS (C) and NiCe (D) .....	48
<b>Figure 4.6.</b> <i>In situ</i> XANES performed in Ce L <sub>III</sub> edge during the SRP reaction using supported nickel catalysts Ni/65CS (A), Ni/75CS (B), Ni/85CS (C) and NiCe (D) .....	49
<b>Figure 4.7.</b> Propane conversion during the SRP at 600 °C over ceria-silica supported Ni catalysts, using a GHSV of 1200 L/g <sub>Cat</sub> .h .....	51
<b>Figure 4.8.</b> Species molar fraction during the SRP at 600 °C over ceria-silica supported Ni catalysts Ni65CS (A), Ni75CS (B), Ni85CS (C) and NiCe (D) using a GHSV of 1200 L/g <sub>Cat</sub> .h .....	52

## Table List

<b>Table 2.1.</b> Carbon formation rate of the supported perovskite systems after the DRM at 1073 K. ....	10
<b>Table 3.1.</b> BET area results and average Ni <sup>0</sup> particle size of the supported perovskite-derived catalysts .....	19
<b>Table 3.2.</b> Average Ni <sup>0</sup> crystallite size growth during the reduction of the supported perovskite precursors at 700 °C .....	22
<b>Table 3.3.</b> Estimated average hydrogen yield considering the fed LPG during different periods of the stability test .....	28
<b>Table 3.4.</b> Carbon formation rate estimated by the TGA analysis of the perovskite-derived catalysts after 24 h of SRLPG reaction .....	31
<b>Table 4.1.</b> BET area results and average Ni <sup>0</sup> particle size of the supported perovskite-derived catalysts .....	42
<b>Table 4.2.</b> Estimated propane reaction rate of ceria-silica supported Ni catalysts at 400 °C .....	53
<b>Table 4.3.</b> Estimated carbon formation rate of the spent ceria-silica supported Ni catalysts .....	53



## AGRADECIMENTOS

Sou grato a todas as pessoas envolvidas com meu projeto ao longo dos desafiadores 4 anos de trabalho. Principalmente, agradeço à minha orientadora por me ajudar a conduzir nosso projeto, da melhor maneira possível; aos meus colegas de laboratório pelo convívio e troca de experiências; e à Faculdade de Engenharia Química por prover o espaço físico e parte dos recursos utilizados nos experimentos. Também sou grato ao professor James J. Spivey e aos meus colegas da Louisiana State University (LSU) pelo trabalho em conjunto, desenvolvido durante o programa de doutorado sanduíche, nos Estados Unidos. Em especial, agradeço aos órgãos de fomento CAPES, CNPq e FAPEMIG pelo apoio financeiro e ao Laboratório Nacional de Luz Sincrotron (LNLS), onde parte das atividades de doutorado foram conduzidas. Por fim, agradeço à minha família por todo apoio, que foi essencial durante os momentos difíceis e obstáculos naturais que surgem ao longo do período de pós-graduação.

## ABSTRACT

The continuous population and economic growth in the world have been a great concern to the scientific community because of the increasing energy demand. Unfortunately, energy generation is still highly dependent on non-renewable raw materials, mainly due to its low cost when compared to renewable energy sources. The environmental impacts caused by non-renewable sources and also the eminent depletion of oil derivatives are the main reasons why mankind looks for diversification in the current energy matrix. In the coming years, it is expected a transition period in which oil products and other polluting energy sources are going to be gradually replaced by renewable raw materials. One way to conduct this transition would be using current technologies to generate renewable energy, such as the production of hydrogen from hydrocarbons. One of several researches in literature for hydrogen production from hydrocarbons is the steam reforming of liquefied petroleum gas (LPG). LPG composition is mostly propane and n-butane, and one of its biggest advantages is that this gas is easily available in several countries, such as Brazil. In order to conduct steam reforming reactions, it is necessary to choose catalysts that have attractive characteristics, such as low cost, high availability in nature, high activity, etc. Regarding the mentioned characteristics, nickel catalysts could be a good alternative for this kind of study. This work aims to evaluate hydrogen production from the steam reforming of LPG using nickel-based catalysts. For this purpose, two main catalytic systems were proposed. In the first one, perovskite type precursors supported on alumina (LaNi/AL) and on ceria-silica (LaNi/CS) were synthesized, as well as an unsupported perovskite (LaNi) for a performance evaluation. In the second catalytic system, four Ni catalysts supported over ceria-silica, with different Ce/Si molar ratios (Ni65CS, Ni75CS, Ni85CS and NiCe) were evaluated. The results showed supported perovskite type precursor led to a better catalytic performance, even though LaNi/AL catalyst presented a relatively high carbon formation rate and LaNi/CS suffered from a slight oxidation of the metallic phase. Supports also played an important role on the supported Ni catalysts performance. It was observed that the higher silica content contributed to the formation of smaller average Ni<sup>0</sup> crystallite sizes, brought a higher thermal resistance to the system and facilitated ceria partial reduction, which provided greater stability and better catalytic performance to Ni65CS.

Key Words: Hydrogen, Steam Reforming, Liquefied Petroleum Gas

## RESUMO

O crescimento populacional e econômico mundial têm sido motivo de bastante atenção devido ao grande aumento da demanda energética, nas últimas décadas. Infelizmente, sabe-se que grande parte da geração de energia ainda é altamente dependente de matérias-primas não-renováveis, principalmente por causa de seu baixo custo, quando comparado às fontes renováveis de energia. Devido aos impactos ambientais causados pela matriz energética atual e também ao seu eminente esgotamento, espera-se que, nos próximos anos, haja um período de transição, no qual derivados de petróleo e outras fontes poluentes de energia sejam gradativamente substituídas por matérias-primas renováveis. Uma das formas de conduzir essa transição seria usando as atuais tecnologias para geração de energias renováveis, como por exemplo, a produção de hidrogênio a partir de hidrocarbonetos. Uma das várias linhas de pesquisa de produção de hidrogênio a partir de hidrocarbonetos consiste na reforma a vapor do gás liquefeito de petróleo (GLP), cuja composição é majoritariamente propano e n-butano e que está facilmente disponível em vários países, como o Brasil. Para conduzir a reação de reforma a vapor é necessário escolher catalisadores que tenham características apropriadas, como baixo custo, alta disponibilidade na natureza, alta atividade, dentre outros. Neste aspecto, catalisadores de níquel se apresentam como uma boa alternativa de estudo. Este trabalho foi elaborado com objetivo de avaliar a produção de hidrogênio a partir da reforma a vapor de GLP, utilizando catalisadores a base de níquel. Para este fim, dois sistemas catalíticos principais foram propostos. No primeiro, sintetizou-se precursores perovskitas suportados em alumina (LaNi/AL) e em céria-silica (LaNi/CS), além de uma perovskita não suportada (LaNi), para efeito de comparação. No segundo, quatro catalisadores de Ni suportados em ceria-silica, com diferentes teores molares de céria foram avaliados (Ni65CS, Ni75CS, Ni85CS e NiCe). Os resultados indicaram que os suportes empregados nas perovskitas foram diretamente responsáveis pelo aumento no desempenho catalítico, apesar de o catalisador LaNi/AL ter apresentado uma relativa alta taxa de formação de carbono e do LaNi/CS ter sofrido uma tênue oxidação da fase ativa. O suporte também desempenhou um papel importante no desempenho dos catalisadores de Ni suportado. Observou-se que o maior teor de sílica proporcionou a formação de menores tamanhos médios de cristalito de Ni<sup>0</sup>, maior resistência térmica ao sistema e facilitado a redução parcial da céria o que proporcionou uma maior estabilidade e melhor desempenho catalítico ao Ni65C.

Palavras chave: Hidrogênio, Reforma a Vapor, gás liquefeito de petróleo

## CHAPTER 1 – INTRODUCTION

Energy generation is a great concern for the next years due to the continuous economic improvement and the increasing in world's population. Bae et al. (2016) reported that in 2010 the primary energy consumption was over three times higher than it was in 1965, especially due to the economic growth of Asian countries, like China and India. For future prospects, Muradov et al. (2008) affirm that by the end of 2025, global power demand will almost double, going from 13 to 23 terawatts. Energy consumption is not only related to economic growth but also to greenhouse gases (GHG) emissions, because most of the energy production is still highly dependent on non-renewable sources, especially fossil fuels. According to the U.S. Department of Energy (DOE) around 85% of energy needs are supplied by non-renewable sources like natural and coal, as can be seen in Fig. 1.1.

**U.S. electricity generation at utility-scale facilities in 2016**

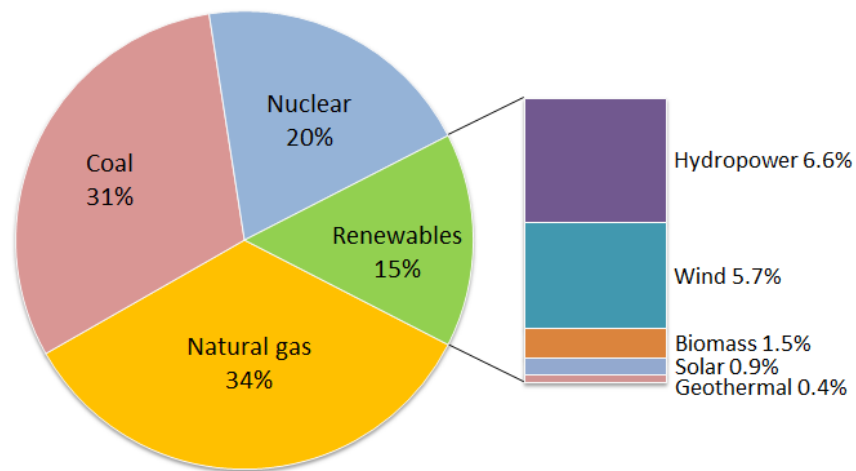


**Figure 1.1:** Energy production sources in the USA (2016).

Many efforts have been done to diversify the global energy matrix and to diminish the production of GHG. Two of the main strategies reported on literature in order to reach this goal are the use of renewable energy resources and the decarbonization of fossil fuels (Muradov et al., 2008). However, a large use of renewable energy sources in short terms is highly improbable. A change on the world's energy matrix may occur gradually in this century mainly due to the depletion of petroleum derivatives sources. In this scenario, it would be interesting to use the well-established technologies to conduct the transition of non-renewable to renewable energy. A good example of this smooth transition is the production of hydrogen using fossil fuels (Izquierdo et al., 2012).

Hydrogen seems to be one of the most promising renewable energy vectors since it has the highest energetic density of all known fuels. Its combustion generates 2.4, 2.8 and 4 times more energy than methane, gasoline and coal, respectively, in a mass basis comparison (Abbas and Wan Daud, 2010). Besides its high calorific value, hydrogen is also environmentally friendly, since it can be produced from renewable feedstock and its combustion does not generate greenhouse gases (Ni et al., 2007). Therefore, hydrogen technologies have drawn much attention to the scientific community and they have been widely studied in literature.

It is important to point out that hydrogen technologies still have to be well developed to be implemented in order to become economically viable in comparison to oil derivatives (LeValley et al., 2014). To accomplish that goal, it would be ideal if hydrogen could be extracted from nature in its gas form, i.e.  $H_{2(g)}$ . Unfortunately, hydrogen gas sources are extremely rare in our planet. Despite being the most abundant element in the universe hydrogen is almost always found as a component of other substances such as water and hydrocarbons. Therefore, it is necessary to extract this element from other feedstock, which makes hydrogen utilization in large scale very expensive yet (Haryanto et al., 2005). Another important economic issue is related to hydrogen storage and transportation. As hydrogen density and ignition energy are very low, not only it is difficult to transport the gas but it also implicates in high risk of explosions. Thus, specific operations such as high-pressure compression and low temperature liquefaction are generally required in order to store and transport this energetic matrix, which enhances costs (Wang et al., 2009).

According to Wang et al. (2009) there are three main processes to produce hydrogen: biological, electrochemical (by water electrolysis) and chemical. The authors affirm that since biological processes have low efficiency and water electrolysis is still very expensive, chemical methods are the best option to produce hydrogen in high scale.

Studies about chemical processes to produce hydrogen such as coal gasification (Li et al., 2010), steam reforming (Schadel et al., 2009; Maluf and Assaf, 2009; Feio et al., 2007), dry reforming (Silva et al., 2012) and partial oxidation (Silva et al., 2005; Hu et al., 2014) of natural gas, can be easily found in literature. Although other chemical processes such as biomass reforming (Borges et al., 2018; Resende et al., 2015) have also been studied in recent years, the mentioned steam reforming of natural gas is still the major responsible for hydrogen production. According to LeValley et al. (2014), around 95% of hydrogen production in the U.S was obtained by the steam reforming of methane (SRM), the main component of natural gas. In this process, methane and steam are converted into hydrogen ( $H_2$ ) and carbon monoxide (CO), when they are exposed to high temperatures, around 800 °C (Equation 1). The produced CO can also react with steam generating

CO<sub>2</sub> and additional H<sub>2</sub> (Equation 2). Equations 1 and 2 combined create a global reaction (Equation 3). These reactions are well established and can be easily found in literature:



In a scenario where methane sources are contaminated with carbon dioxide and the separation process is impracticable, dry reforming of methane (DRM - Equation 4) could be an alternative to SRM. However, there is one major problem associated to dry reforming that must be taken into account. Oyama et al. (2012) shows that DRM is always associated with the reverse water-gas shift (RWGS) reaction (Equation 5), which consumes part of the produced hydrogen to form water. This undesirable fact does not occur with SR because the associated reaction is the latter mentioned WGS, which has the opposite effect: it contributes to produce more hydrogen.



Although the SR of natural gas is the main responsible for H<sub>2</sub> production in the world, this process is still undoable in remote places such as the interior of some countries, especially because in those areas natural gas pipelines are usually not available. In this cases LPG (liquefied petroleum gas) could be a good candidate to produce hydrogen since it can be easily transported and stored on-site (Laosiripojana et al. 2010). In some countries like Brazil, there is already a well-established distribution infrastructure of LPG, since this gas is widely used for cooking, even in remote areas. Therefore using LPG to produce hydrogen becomes even more attractive due to its effective cost and easy distribution (Silva et al., 2017; Faria et al., 2016).

This work aims the study hydrogen production from steam reforming of LPG using two different nickel catalytic systems. In order to reach this goal, our study was divided into five main chapters, which are a brief introduction of the subject (Chapter 1), a general literature review (Chapter 2) and the results obtained from the proposed catalytic systems (Chapters 3 and 4).

Chapter 3 describes the results of the characterization tests of perovskite type precursors and their performance during the steam reforming of LPG. In this catalyst series, three perovskite type precursors were synthesized. One was supported on alumina (LaNi/AL), another on ceria-silica

(LaNi/CS), and the third one was analyzed unsupported (LaNi) for comparison purposes. The performance tests were conducted at both 600 and 700 °C and the characterization tests of the catalysts were BET area, *in situ* XRD, *in situ* XANES and TGA.

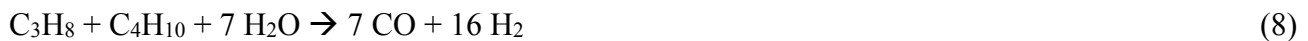
Chapter 4 approaches our study on four ceria-silica supported nickel precursors. The catalysts were synthesized with the same amount of Ni (10%wt), which was supported over ceria-silica materials with different ceria molar content.

Further details about the catalyst's performance and characterization tests will be explored on these specific chapters.

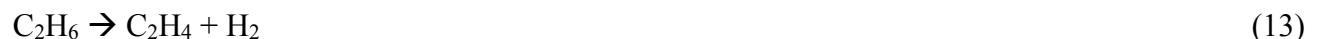
## CHAPTER II – LITERATURE REVIEW

The objective of this chapter was to give a small sample of the studies already published in literature and to introduce the reader to the subject. In the following chapters, more specific studies used to discuss the findings about each catalytic system will be presented.

LPG is a mixture of hydrocarbons, mainly propane and butane with different ratio compositions, which vary according to the exploration source of this gas (Raslavičius et al., 2014; Laosiripojana et al. 2011). Thus, there are different studies in literature that carry out hydrogen production by the steam reforming of LPG (SRLPG) using propane (Harshini et al., 2012), butane (Jeong and Kang, 2010) or both (Silva et al., 2017) as model molecules of this gas. Equations 6, 7 and 8 show the steam reforming reaction of this systems, respectively.



The main products formed in the SRLPG are  $\text{H}_2$ ,  $\text{CO}$  and  $\text{CO}_2$ . However, it is also observed the formation of ethane, ethylene, methane and specially coke in this process due to undesired reactions, such as the Boudouard reaction, methanation and decomposition of propane and butane, which usually happen in parallel. Faria et al. (2016) and Laosiripojana et al. (2010) have reported some of these reactions that can be seen through Equations 9 to 15.



In literature, it is possible to find some thermodynamic analysis of hydrogen production from LPG reforming. In order to study the behavior of this systems most of the cited reactions (Equations



1 to 15) are considered. Wang et al. (2010) performed a thermodynamic study of the steam (SRP) and dry (DRP) reforming of propane employing free Gibbs energy minimization to do equilibrium calculations. The analysis was carried out considering a variation range of pressure (1 to 5 atm), temperature (700 to 1100 K), water to propane ratio (1 to 18) and carbon dioxide to propane ratio (1 to 12). The authors concluded that the DRP produces a synthesis gas with low hydrogen content, while the SRP had the opposite effect, generating a rich hydrogen content. This result is in accordance to Oyama et al. (2012) study, which explains the negative effect of the RWGS reaction in dry reforming processes for hydrogen production. Wang et al. (2010) also concluded that an optimum condition for hydrogen production from the SRP occur in atmospheric pressure, temperatures between 925 and 975 K and a water to propane ratio between 12 and 18. Under these conditions, methane and carbon formation were negligible. Figure 2.1 shows the number of  $H_2$  moles produced per mole of propane, as a function of temperature and water to propane ratio (WPR).

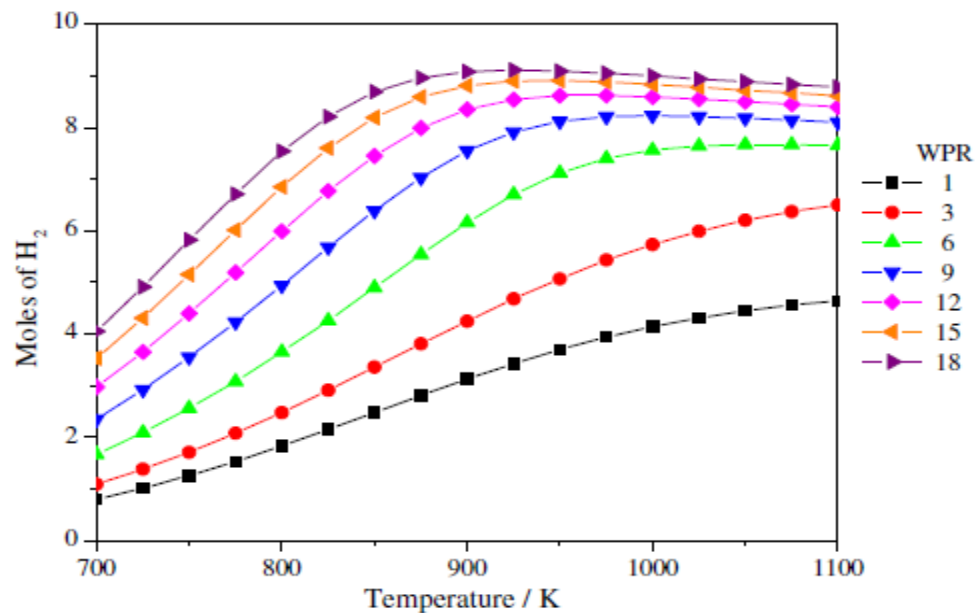


**Figure 2.1:** Moles of hydrogen produced per mol of reacted propane, as a function of temperature and WPR at atmospheric pressure.

In order to perform the steam reforming reactions of LPG it is essential to select adequate catalysts. Some characteristics as reasonable cost, low carbon formation rate, high activity and stability are greatly required (LeValley et al., 2014). There are some studies in literature that use noble metals such as Rh (Laosiripojana et al., 2011), Pd (Faria et al., 2008), Ru (Alvarez-Galvan et

al., 2011) and Pt (Gokaliler et al., 2012) as catalytic precursors in the steam reforming of LPG, propane or butane. However, noble metals are known to be expensive and considerable scarce in the nature (Zhang et al., 2009), which make them impracticable in a large-scale process of producing hydrogen.

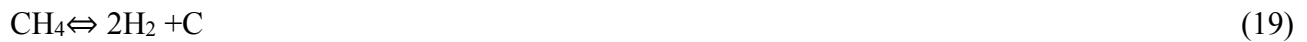
Otherwise, nickel is easily available in nature and considerably cheaper than noble metals. Besides, Ni catalysts favor bonding breaking C-C and C-H which is highly required in the steam reforming of hydrocarbons (Roh et al., 2003). Although Ni catalysts have some advantages, it is important to point out that there are four major issues associated with the use of nickel catalysts for steam reforming processes. The first one is the deactivation of Ni catalysts caused by sulfur contamination. Sulfur, which is present in many sources of natural gas and LPG, poisons Ni catalysts by blocking their active sites with H<sub>2</sub>S. The second important issue is that Ni catalysts are difficult to activate. Thus, they require more energy and consequently a higher activation temperature, which leads to the third major problem: sintering. Sintering is a phenomenon that causes a particles' size growth by their aggregation, which diminishes the number of active sites and lowers activity. At last, Ni catalysts suffer from carbon formation, which also causes the block of active sites, increases pressure drop, and decreases heat transfer (LeValley et al., 2014)

In order to minimize carbon deposition and particles sintering, it is very important to choose adequate supports in a Ni based catalytic system, since it affects directly the dispersion, superficial area and stability of the catalysts (Nogueira et al., 2014; Hu and Lu, 2010).

Ceria-based supports are widely used for a variety of hydrocarbon reactions to produce hydrogen. These materials have some desirable characteristics that make their use in steam reforming systems more attractive. Among them, it is important to emphasize the high oxygen storage capacity and oxygen mobility of these materials, since they favor the mechanism of carbon removal and increase the catalyst stability. Besides this mechanism, the strong interaction with the metallic phase of the system (metal-support interaction) also helps the stabilization of the catalyst. Another characteristic that is highly important to be mentioned is ceria redox property between Ce<sup>4+</sup>/Ce<sup>3+</sup> since it helps the surface oxidation and consequently favors the reactions between carbon species and the lattice oxygen of the material (Liu et al., 2011; Laosiripojana et al., 2011).

Laosiripojana and Assabumrungrat (2006) reported a comparative between a Ni/Al<sub>2</sub>O<sub>3</sub> and two CeO<sub>2</sub> systems during the steam reforming of propane at 900 °C. This work shows coking issues that are commonly observed when Ni based catalysts are used to perform this kind of reaction. The authors concluded that Ni/Al<sub>2</sub>O<sub>3</sub> suffered from high deactivation due to high carbon deposition rate,

which was significantly lower in CeO<sub>2</sub> catalytic systems. The authors also reported possible carbon formation routes, which are described by Equations 16 to 22.



Although ceria has considerable advantages in steam reforming processes, there is a major issue associated to its use that must be taken into account: the low thermal stability of this material. When exposed to high temperatures ceria particles suffer from sintering, which can diminish its oxygen storage capacity and low the catalyst activity (Reddy et al., 2003). In order to increase thermal stability, some dopants as SiO<sub>2</sub>, ZrO<sub>2</sub> and TiO<sub>2</sub> can be added to ceria materials. The incorporation of dopants into ceria forms a mixed oxide phase, which alters the electronic structure of the cations and increases lattice defects, since they cause an instability of Ce<sup>4+</sup>-O bonds. This phenomenon improves oxygen reactivity due to an increase in oxygen transfer rates, which causes an enhancement on the precursor's reducibility (Ribeiro et al., 2013; Liu et al., 2011).

Faria et al. (2016) investigated the influence of ceria-zirconia Ce<sub>x</sub>Zr<sub>1-x</sub>O<sub>2</sub> (x = 0.5, 1) on Ni catalysts over alumina during the steam reforming of LPG. The authors observed that even though Zr doping had a beneficial effect on the catalyst activity when compared to Ni/Al<sub>2</sub>O<sub>3</sub>, Ni/CeO<sub>2</sub>/Al<sub>2</sub>O<sub>3</sub> still had a better performance. The authors also showed that Ni/Al<sub>2</sub>O<sub>3</sub> suffered from deactivation due to carbon deposition while the catalysts supported over ceria and ceria-zirconia did not have the same problem.

Yap et al. (2013) studied the DRM using Ni catalysts supported on the binary CeO<sub>2</sub>-SiO<sub>2</sub> with different ceria loadings. The authors observed that the catalysts supported over ceria-silica showed a better performance and a lower carbon formation rate than Ni/SiO<sub>2</sub> and Ni/CeO<sub>2</sub>. Hu et al. (2014) used supported Ni catalysts over x.CeO<sub>2</sub>-(1-x).SiO<sub>2</sub> (x = 0, 0.25, 0.50, 0.75, 1) during the partial oxidation of methane. It was observed that the highest methane conversion was obtained over the catalyst with Ce/Si molar ratio of 1:1. This catalyst also presented a good stability and remained active during 900 min reaction.

Another alternative to diminish carbon deposition and particles sintering phenomena is to use structured compounds as catalytic precursors. Highly dispersed particles can be obtained by the destruction of a structured compound, which helps not only to avoid particles agglutination but also to decrease the carbon formation rate (Lima et al., 2010). A recurrent example of structured compound reported on literature are perovskite-type precursors, which have a cubic structure and the empirical formula of  $ABO_3$ . In this formula, A generally corresponds to a rare-earth metal, which occupies the center atom of the cubic structure and B corresponds to a transition metal, which is the metallic active site of the precursor. This structure is destroyed upon reduction forming a highly dispersed B metallic phase on a matrix  $A_2O_3$  (Johansson et al., 2014). A schematic figure of a perovskite-type precursor can be seen in Fig. 2.2.

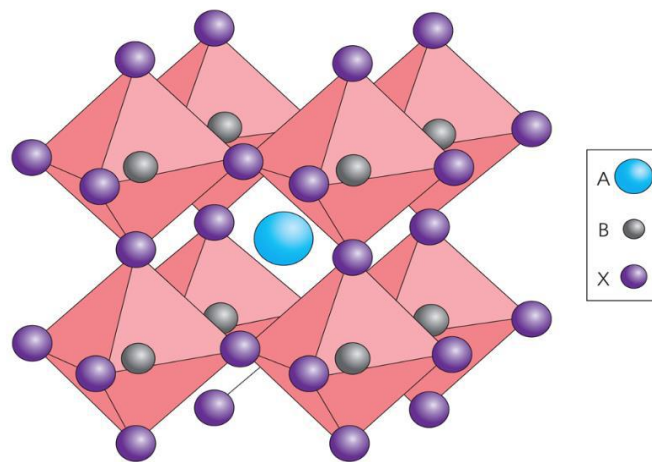


**Figure 2.2:** Theoretical scheme of a perovskite structure.

There are some works in literature that use Ni perovskite-types precursors to perform the steam reforming of hydrocarbons in order to study not only their activity but also their resistance towards carbon deposition. Silva et al. (2017) conducted an investigation of the effect of doping (Sr and Ce) metals in the perovskite structure during the steam and oxidative reforming of LPG. The authors observed that at 873 K all precursors suffered from high deactivation by carbon deposition, even when a small amount of oxygen was added to the system in order to attenuate this issue. On the other hand, at 973 K the catalysts showed a considerable better performance and when the temperature was risen up to 1073 and 1173 K it was possible to maintain the activity of the catalysts, which reached 100% of LPG conversion, during 24 h of reaction. The authors also reported that the perovskite doped with Ce, i.e  $La_{0.95}Ce_{0.05}NiO_3$ , presented the best catalytic performance. They

attributed this result to a smaller Ni particle size of this sample, but also to the presence of cerium that favors the mechanism of carbon removal. The mentioned results can be seen in Fig. 2.3.

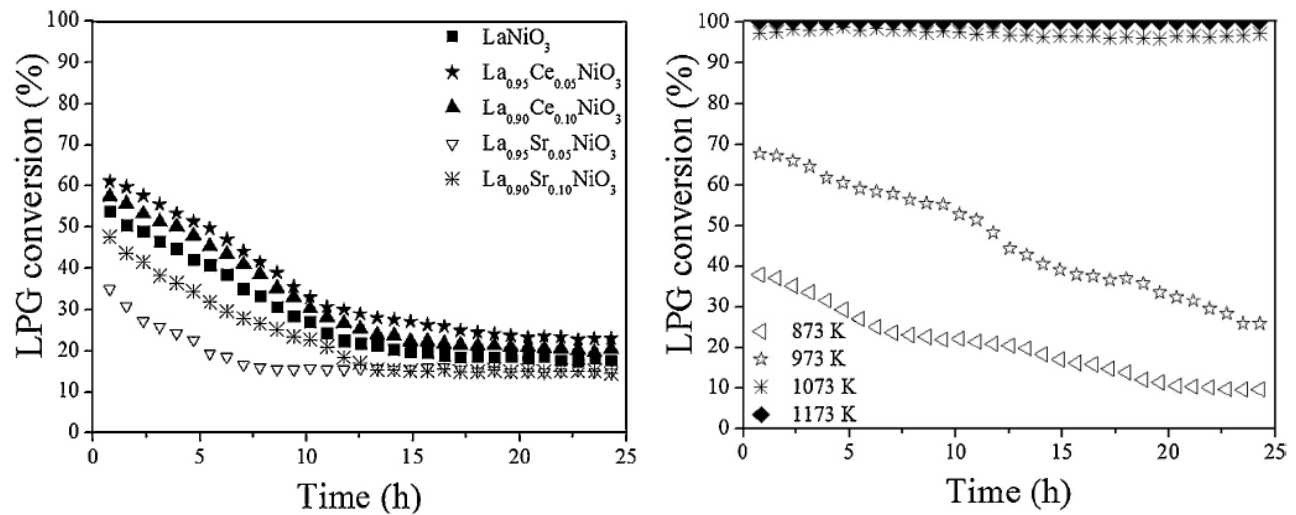


**Figure 2.3:** (A) LPG conversion of perovskite-derived catalysts at 873 K (B) LPG conversion at different temperatures using  $\text{La}_{0.95}\text{Ce}_{0.05}\text{NiO}_3$  catalyst during the steam reforming process. Feed Condition:  $\text{LPG}/\text{H}_2\text{O} = 1/7$ ;  $\text{W}/\text{F} = 0.05 \text{ mg}\cdot\text{min}/\text{L}$  (Silva et al., 2017)

Rabelo-Neto et al. (2018) investigated the influence of supports in a perovskite catalytic system during the dry reforming of methane (DRM). Three perovskite-type precursors were used: a supported  $\text{LaNiO}_3$  over alumina ( $\text{LaNiO}_3/\text{Al}_2\text{O}_3$ ), a supported  $\text{LaNiO}_3$  over a silicon doped ceria ( $\text{LaNiO}_3/\text{CeSiO}_2$ ) and a non-supported  $\text{LaNiO}_3$ , used for comparison effects. According to the authors supporting perovskite-type oxides over materials with a high surface area such as alumina and a ceria-mixed oxide could diminish carbon deposition rates. The supports would have the role to increase Ni dispersion and to provide oxygen to the metallic surface, which prevents carbon accumulation. During the analysis the authors observed that  $\text{LaNiO}_3$  catalyst exhibited the lowest initial conversion, which continuously increased during the reaction until the experiment was stopped due to a strong pressure drop in the system.  $\text{LaNiO}_3/\text{Al}_2\text{O}_3$  also presented a conversion raise, but after 4 h of reaction it stabilized and stood around 60% for methane. On the other hand,  $\text{LaNiO}_3/\text{CeSiO}_2$  showed a stable conversion rate during 24 h reaction. A comparison among  $\text{LaNiO}_3$ ,  $\text{LaNiO}_3/\text{Al}_2\text{O}_3$  and  $\text{LaNiO}_3/\text{CeSiO}_2$  activities can be seen in Fig. 2.4.

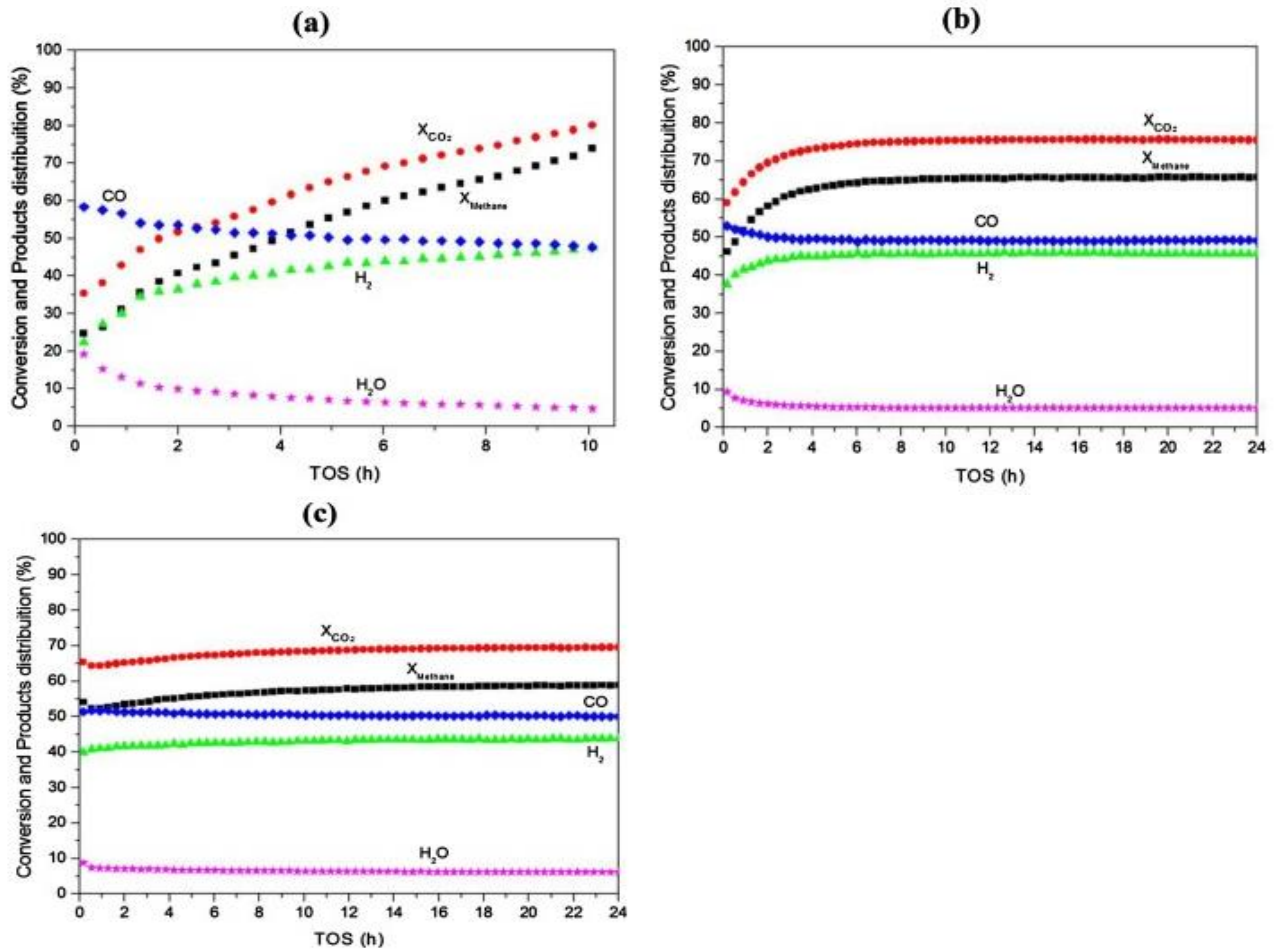


**Figure 2.4:** Methane and  $CO_2$  conversion versus TOS for DRM at 1073 K and  $CH_4/CO_2 = 1.0$  over (a)  $LaNiO_3$ ; (b)  $LaNiO_3/Al_2O_3$ ; (c)  $LaNiO_3/CeSiO_2$  (Rabelo-Neto et al., 2018).

After the analysis Rabelo-Neto et al. (2018) concluded that  $CeSiO_2$  practically inhibited carbon deposition over the metallic phase due to the OSC of the support that does not favor the mechanism of carbon formation. Table 2.1 shows the different carbon formation rates among their three catalysts.

**Table 2.1:** Carbon formation rate of the supported perovskite systems after the DRM at 1073 K.

Catalyst	Reaction conditions	mgC/g <sub>cat</sub> *h
$LaNiO_3$	T = 1073 K, $CH_4:CO_2 = 1:1$	27.04
$LaNiO_3/Al_2O_3$	T = 1073 K, $CH_4:CO_2 = 1:1$	7.58
$LaNiO_3/CeSiO_2$	T = 1073 K, $CH_4:CO_2 = 1:1$	0.32

The authors concluded that the lack of coke enhanced the catalyst activity and concede more stability to the system. Supporting the perovskite-type oxide over alumina also contributed to diminish the carbon formation rate, which was around one third of the non-supported  $\text{LaNiO}_3$ .

Although many works report the effects of Ni supported catalysts during the steam reforming of hydrocarbons, there are no studies using supported perovskites as a catalytic system during the steam reforming of LPG. Therefore, this work aims to study the steam reforming of liquefied petroleum gas (LPG) using supported Ni catalysts. Propane or a propane-butane mixture will be used as model molecules of LPG. Two catalytic systems were proposed to the analysis: Ni supported over ceria-silica  $x.\text{CeO}_2-(1-x).\text{SiO}_2$  ( $x = 0.65, 0.75, 0.85$  and  $1$ ) and supported Ni perovskites ( $\text{LaNiO}_3$ ,  $\text{LaNiO}_3/\text{Al}_2\text{O}_3$  and  $\text{LaNiO}_3/\text{CeO}_2\text{-SiO}_2$ ).

## **CHAPTER 3 - HYDROGEN PRODUCTION FROM THE STEAM REFORMING OF LPG USING SUPPORTED PEROVSKITE PRECURSORS.**

**ABSTRACT** - Perovskites supported over  $\text{Al}_2\text{O}_3$  (LaNi/AL) and  $\text{CeO}_2\text{-SiO}_2$  (LaNi/CS) were evaluated as catalysts for steam reforming of liquefied petroleum gas (SRLPG), aiming the production of hydrogen. A non-supported  $\text{LaNiO}_3$  was also synthesized for comparison effects. *In situ* X-Ray Diffraction analyses pointed out that temperature reduction of 700 °C was enough to generate  $\text{Ni}^0$  and  $\text{La}_2\text{O}_3$ , except for LaNi/AL. This could be due to  $\text{NiAl}_2\text{O}_4$  and  $\text{LaNi}_{0.5}\text{Al}_{0.5}\text{O}_3$  phases which granted a high thermal stability to this precursor. X-Ray absorption Near Edge Spectroscopy (XANES) showed a direct influence of the supports in the reduction temperature. It was noticed that supported precursors maintained better catalytic activity during SRLPG reaction at 600 °C. Stability test results at 600°C showed that alumina support provided a high performance to LaNi/AL mainly due to the strong metal-support interaction. At 700 °C, LaNi/CS presented LPG conversion reaching almost 100%. At both temperatures, the lowest carbon accumulation rate was obtained by LaNi/CS probably due to ceria oxygen mobility.

Keywords: Perovskite, LPG, Hydrogen.

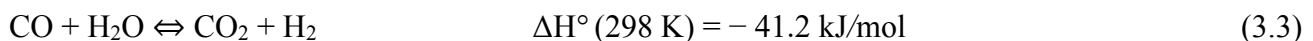
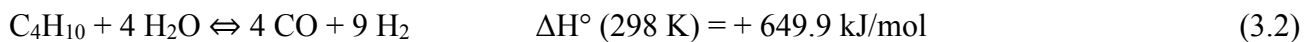
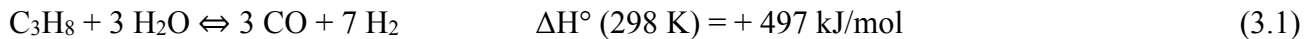


### 3.1. Introduction

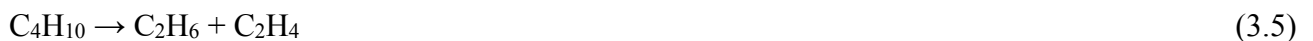
Hydrogen is an environmentally friendly fuel since its combustion only generates water as a sub product. It can also be produced by renewable feedstocks as biomass, which has neutral carbon energy supply (Vagia and Lemonidou, 2008). However, renewable resources are not enough to guarantee a steady supply of hydrogen nowadays. Hence, it is still necessary to use fossil fuels such as natural gas, GLP, nafta and others to fulfill its demand, even though it is unsustainable in long terms (LeValley et al., 2014).

According to Jeong and Kang (2010) the expansion of hydrogen economy has raised the interest in studying the steam reforming of light hydrocarbons, such as propane and butane. The authors affirm that LPG has considerable advantages over other compounds since it can be easily handled, transported and stored. Besides, many cities already have an existing infrastructure for LPG, normally destined for heating and cooking (Silva et al., 2017), which makes LPG a promising fuel to generate hydrogen on-shore (Avci et al., 2001).

Steam reforming reactions of propane and butane can be described by Equations 3.1 and 3.2, respectively, as well as the water gas shift reaction (Equation 3.3) that currently occurs simultaneously with the latter ones (Malaibari et al., 2014, Avci et al., 2004):



The main products of the steam reforming of LPG are carbon monoxide, carbon dioxide and hydrogen. However, undesirable products can also be formed by decomposition (Equations 3.4 and 3.5) and methanation (Equation 3.6, 3.7 and 3.8) reactions such as methane, ethane and ethylene (Silva et al., 2017; Avci, 2004).



To perform successfully the steam reforming of LPG it is necessary to develop catalysts with propitious characteristics to the process such as high activity, good selectivity for the desired products and low cost. Therefore, nickel-based catalysts are a good choice since they could lead to all the required attributes. However, nickel might suffer from deactivation, mainly by particles sintering and coking. Sintering is generally associated to severe process conditions such as high temperatures. Coking is always a great concern for Ni based catalysts, especially when they are exposed to higher carbon chain compounds as propane and butane, since it may cause considerable drop in the catalytic performance (Malaibari et al., 2014; Oemar et al., 2013). Some of the most common coke generation routes that may occur as parallel reactions during the steam reforming of LPG are described from Equation 3.9 to 3.14, as follows (Laosiripojana and Assabumrungrat, 2006):



To minimize Ni deactivation by coking it might be a good idea to use structured compounds as catalytic precursors like perovskites, since the destruction of this compound generates relatively high dispersed particles and consequently smaller average Ni crystallites. Perovskites are mixed oxides represented by the formula  $\text{ABO}_3$ , in which A is an alkali, alkaline earth or rare earth metal and B is a transition metal. The A metal normally promotes stability and catalyst activity, while the B metal provides the catalyst active sites (Choi et al., 2009).

Perovskite-based Ni catalysts generally have good catalytic properties for dry or steam reforming of hydrocarbons in terms of activity, coke resistance and thermal stability (Rivas et al., 2010). Thus, there are plenty of studies portraying the use of nickel in perovskite precursors during steam reforming processes in the literature. Pereniguez et al. (2010) studied the synthesis and characterization of  $\text{LaNiO}_3$  perovskite-type precursors during the steam and dry reforming of methane. During their experiments the authors observed remarkable stability of the catalyst under dry reforming conditions, which they attribute to high oxidation resistance of the Ni particles. The same behavior was not noticed under the steam reforming condition as the catalyst suffered a gradually oxidation due to the presence of water and consequently had a considerable performance

decrease. Silva et al. (2017) have investigated the doping effect of Cerium and Strontium in perovskites as precursors for steam and oxidative reforming of LPG at 873 and 973 K. Results showed that all catalyst suffered from strong deactivation due to coke deposition at the lower temperature while at the higher one, it was possible to maintain a stable catalytic activity and hydrogen production.

Nevertheless, perovskites have low superficial area which could limit their application in catalysis. So, it would be interesting to use them associated with other materials as supports not only to enhance catalytic activity (Rivas et al., 2010) but also to avoid carbon formation. There are some advantages in the use of lanthanides as promoters as they not only can diminish coking but also help maintaining catalyst activity (Zhang et al. 2009).

Literature shows that ceria is able to promote the active phase of various metals mainly due to the high oxygen store capacity and mobility of this material (Laosiripojana and Assabumrungrat, 2006). Furthermore,  $\text{CeO}_2$  can promote water gas shift and steam reforming reactions (Reddy and Khan, 2005). Although ceria has a wide range of applications its use as a pure material is discouraged since  $\text{CeO}_2$  has low thermal stability. Thus, the exposure of ceria to high temperatures, like the ones needed for reforming processes, could cause a sintering of its particles and consequently affect its oxygen storage and release capacity (Reddy et al., 2003).

In order to concede a higher thermal stability to ceria, other materials that are extensively employed as supports such as  $\text{SiO}_2$  and  $\text{ZrO}_2$  could be combined to it. Rabelo-Neto et al. (2018) studied perovskites supported over  $\text{CeO}_2\text{-SiO}_2$  and  $\text{Al}_2\text{O}_3$  during the dry reforming of methane performed at  $800^\circ\text{C}$ . A non-supported  $\text{LaNiO}_3$  was also evaluated for comparison purposes. The authors affirmed that  $\text{LaNiO}_3$  presented the lowest initial conversion which indicates a clear influence of the supports on the catalytic activity. They also concluded that the significant drop on carbon deposition observed in  $\text{LaNiO}_3/\text{CeSiO}_2$  catalyst was due to the high oxygen storage/release capacity of the  $\text{CeO}_2\text{-SiO}_2$  support. However, studies about supported perovskites are still scarce in literature. There are not any works that show the effect of supported perovskites as catalytic precursors in the steam reforming of LPG. Thus, the aim of this work is to evaluate the influence of different types of supports ( $\text{Al}_2\text{O}_3$  and  $\text{CeO}_2\text{-SiO}_2$ ) in the performance of perovskite precursors during the steam reforming of LPG.

## 3.2. Methodology

### 3.2.1. Catalyst preparation

Three perovskite-type precursors were prepared using sol-gel method: a non-supported perovskite ( $\text{LaNiO}_3$ ); a ceria-silica supported perovskite ( $\text{LaNiO}_3/\text{CeO}_2\text{-SiO}_2$ ); and an alumina supported perovskite ( $\text{LaNiO}_3/\text{Al}_2\text{O}_3$ ). They were named as LaNi, LaNi/CS and LaNi/AL, respectively.

To prepare the non-supported  $\text{LaNiO}_3$ , stoichiometric quantities of  $\text{La}(\text{NO}_3)_3 \cdot 6\text{H}_2\text{O}$  (99%, Vetec) and  $\text{Ni}(\text{NO}_3)_2 \cdot 6\text{H}_2\text{O}$  (97%, Vetec) were dissolved in deionized water to obtain a 1.0 mol/L solution. This solution was homogenized under stirring during 30 min at 70 °C. Then, a solution containing citric acid (99.5%, Dinâmica) and ethylene glycol (99.5%, Dinâmica) was added to the solution of nitrates precursors to obtain a molar proportion of 1:1:1. After 4 h of vigorous stirring at 70 °C, it was obtained a viscous material that was dried in a stove at 110 °C for 12 h. The resulting material was macerated and calcined under air flow (50 mL/min) at heating rate of 5 °C/min from 25 to 800 °C, remaining at this temperature for 10 h.

The same procedure was adopted to prepare supported perovskite samples. All the calculations were performed to obtain supported samples containing 30 wt% of  $\text{LaNiO}_3$ , which corresponds to 7 wt% of Ni, approximately. The appropriated amounts of  $\text{La}(\text{NO}_3)_3 \cdot 6\text{H}_2\text{O}$  (99%, Vetec) and  $\text{Ni}(\text{NO}_3)_2 \cdot 6\text{H}_2\text{O}$  (97%, Vetec) were dissolved in water to obtain a 1.0 mol/L solution, which was kept under stirring at 70 °C for 30 min. The desired support (alumina or ceria-silica) was then added to this solution and homogenized. Before the supports addition, each of them was calcined over 800 °C during 6 h. Then, a solution containing citric acid (99.5%, Dinâmica) and ethylene glycol (99.5%, Dinâmica) was added to obtain a molar proportion of 1:1:1. These final mixture was kept under stirring for 4 h at 70 °C. The obtained material was dried and calcined in the same conditions used for  $\text{LaNiO}_3$  sample.

Commercial alumina (Puralox-Sasol) and  $\text{SiO}_2$  (Aerosil 200 – Degussa) were used on the supports.  $\text{CeO}_2\text{-SiO}_2$  support was prepared dissolving the calcined  $\text{SiO}_2$  (Aerosil 200 – Degussa) in an alkaline solution containing potassium hydroxide. The resulting solution was added to another one of ammonium hydroxide. Then, the precipitation process was performed by adding a solution of  $(\text{NH}_4)_2\text{Ce}(\text{NO}_3)_6 \cdot 6\text{H}_2\text{O}$  (Aldrich 98%). After that, the precipitate was kept under stirring for 30 min, washed with water until its pH become neutral ( $\text{pH} = 7.0 \pm 0.5$ ) and dried for 12 h at 110 °C in a muffle. The material was heated to 800 °C at a heating rate of 10 °C/min and maintained at this temperature for 5 h under air flow. The  $\text{CeO}_2\text{-SiO}_2$  support has a Ce/Si molar ratio of 3.0.

### 3.2.2. Characterization

#### 3.2.2.1. BET Area

BET surface areas of the samples were measured using a thermal conductivity detector (QUANTASORB JR) by nitrogen adsorption at  $-195\text{ }^{\circ}\text{C}$ . Before the analysis, all samples were dried in He flow at  $150\text{ }^{\circ}\text{C}$ , for 12 h.

#### 3.2.2.2. *In situ* X-Ray Diffraction (XRD)

*In situ* XRD was performed at the D10B-XPD beamline at LNLS in Campinas-BRAZIL. A wavelength of  $1.5498\text{ \AA}$  at 8 keV was used. The scanning of each sample was done in a  $2\theta$  range from  $22$  to  $58^{\circ}$ , with  $0.003^{\circ}$  step and 1 s of counting time. All samples were reduced using a gas mixture of 5%  $\text{H}_2$ :He, with a 100 mL/min flow rate and a heating rate of  $10\text{ }^{\circ}\text{C}/\text{min}$  from  $25$  to  $700\text{ }^{\circ}\text{C}$ , keeping this temperature for 2 h. The average crystallite sizes were evaluated by Scherrer equation using the line characteristic of  $\text{Ni}^0$  at  $2\theta = 51.8^{\circ}$ , after the reduction process.

#### 3.2.2.3. X-Ray Absorption Near Edge Structure (XANES)

XANES experiments were conducted at DXAS beamline at LNLS (Laboratório Nacional de Luz Síncrotron) in Campinas - BRAZIL. X-ray absorption data of each sample was collected monitoring the Ni K-edge ( $8333\text{ eV}$ ) during a reduction procedure. XANES data was also collected in the  $\text{L}_{\text{III}}$  Ce-edge ( $5723\text{ eV}$ ) for LaNi/CS sample, during the reduction. The samples were reduced under a 5%  $\text{H}_2$ :He mixture (100 mL/min) using a heating rate of  $10\text{ }^{\circ}\text{C}/\text{min}$  from  $25$  to  $700\text{ }^{\circ}\text{C}$  and kept in  $700\text{ }^{\circ}\text{C}$  for 2 h. Software ATHENA/IFEFFIT was used to treat XANES data. All spectra were normalized using standard proceedings.

### 3.2.3. Catalytic Performance

Stability tests were conducted at  $600$  and  $700^{\circ}\text{C}$ , during 24 h using a fixed bed reactor. 10 mg of LaNi precursor and 33 mg of the supported precursors (LaNi/AL and LaNi/CS) were mixed with 123 mg and 100 mg of quartz (used as an inert), respectively. Different amounts of supported and non-supported samples were used aiming to obtain the same amount of metallic Ni sites. The mixture of precursor and inert was charged into a quartz tube reactor and reduced with  $\text{H}_2$  (30 mL/min) at  $700\text{ }^{\circ}\text{C}$  for 2 h. Propane and butane were fed at a 10 mL/min flow rate each. Water was pumped continuously into heated lines where it was vaporized at  $150\text{ }^{\circ}\text{C}$  and carried with 44 mL/min

flow of argon into the reactor maintained at 600 or 700 °C. The effluent gases were analyzed using gas chromatography (GC-2014, SHIMADZU) with TCD (column Carboxen 1010) and FID (column Rt-QPLOT) detectors. LPG conversion and the dry molar fractions of all species ( $y_i$ ) were calculated according to the following equations:

$$X_{LPG} = \frac{F_{LPG}^{in} - F_{LPG}^{out}}{F_{LPG}^{in}} \quad (3.15)$$

$$y_i = \frac{F_i}{\sum F_i} \quad (3.16)$$

Where  $F_i$  is the molar flow rate of  $i$  species at the inlet or at the outlet of the reactor.

#### 3.2.4. Thermogravimetric Analysis (TGA) after reaction

TGA was performed to quantify the amount of carbon deposited during the SR of LPG reaction. The analysis was done using a SDT Q600 (TA instrument) equipment. All samples were heated from room temperature to 1000 °C in air atmosphere, using a 10 °C/min heating rate. TGA results indicated the mass loss of the samples, which corresponds to the amount of carbon deposited during each reaction. A carbon formation rate ( $R_C$ ) was estimated dividing the mass of solid carbon ( $mg_{C(s)}$ ) by the product of the catalyst mass ( $g_{Cat}$ ), reaction time ( $t$ ) and the reacted carbon mass ( $mg_{C_{reac}}$ ) of each stability test. The main goal of considering the latter is to measure how much of the reacted carbon turned into coke and thus to establish a more fair comparison among the catalysts.

$$R_C = \frac{mg_{C(s)}}{(g_{Cat} \cdot t \cdot mg_{C_{reac}})} \quad (3.17)$$

### 3.3 Results and Discussion

#### 3.3.1 Catalysts Characterization

BET surface area data are reported in Table 3.1. The results showed that the use of alumina support provided a considerable increase in the surface area of the derived-perovskite catalysts. Unfortunately, the same improvement was not observed for the sample supported on ceria-silica. The average Ni crystallite size of each catalyst after reduction at 700 °C was estimated using the Scherrer equation and are also shown in Table 3.1. The calculations were made using *in situ* XRD data and considering  $2\theta = 51.8^\circ$ , since this peak has no interference from other phases of the catalytic system. All the catalysts exhibited approximately the same Ni crystallite size, except for LaNi/CS that has a slightly smaller Ni crystallite size. According to the results, it is possible to affirm that samples LaNi and LaNi/AL have similar average Ni crystallite sizes, so that this parameter would not be suitable to explain possible differences between their catalytic activities. On the other hand LaNi/CS presented the smallest average particle size, which could lead to lower carbon formation rate and consequently an improvement on its catalytic activity (Lima et al., 2010; Trimm, 1997; Rostrup-Nielsen, 1984).

**Table 3.1:** BET area results and average Ni<sup>0</sup> particle size of the supported perovskite-derived catalysts.

Samples	BET Area (m <sup>2</sup> /g)	D <sub>p</sub> Ni <sup>0</sup> (nm)
LaNi	1	22
LaNi/CS	4	15
LaNi/AL	69	23

Fig. 3.1 shows the diffractograms of LaNi (A), LaNi/CS (B) and LaNi/AL (C) samples at room temperature and during reduction under a 5%H<sub>2</sub>/He mixture from 25 °C to 700 °C. The diffractograms of LaNi calcined sample at room temperature show the characteristic diffraction patterns of LaNiO<sub>3</sub> phase at  $2\theta$  equal to 23.3, 32.8, 33.3, 47.5 and 58.6° (ICSD – 67714) in Fig. 3.1A. Another perovskite phase (La<sub>4</sub>Ni<sub>3</sub>O<sub>10</sub>) was also observed at  $2\theta$  equal to 32.3° and 58.5° in this sample. This phase was also reported by Silva et al. (2017) and Resende et al. (2015). NiO phase was detected at room temperature for this sample, as well as, for the other supported perovskites, which agrees well with the incomplete formation of the LaNiO<sub>3</sub> phase. In Figure 3.1A, as the

temperature is increased and the reduction process starts, it is possible to observe that the perovskite structures were destroyed forming the characteristic Ni<sup>0</sup> diffraction patterns observed at 2θ equal to 44.1 and 51.8° (ICSD – 260169). However, NiO phase (2θ equals to 37.2°, 43.3° and 62.9° (ICSD: 9866)) that was detected at room temperature also had a contribution in the amount of reduced nickel. Another strong evidence of perovskite structure destruction is the presence of La<sub>2</sub>O<sub>3</sub> peaks at 2θ equal to 26.1, 29.1, 30.0, 39.5, 46.1, 55.4 and 55.9° (ICSD – 100204) in the diffractograms at 700 °C (2 h). This result is in agreement with previously data reported in the literature (Lima et al. 2010, Silva et al. 2017).

For calcined LaNi/CS (Figure 3.1B) at room temperature, the overlapping of lines characteristic of LaNiO<sub>3</sub> phase with the ones characteristic of ceria phase prevented the identification of the presence of LaNiO<sub>3</sub> phase. Cerium silicate (Ce<sub>4.67</sub>Si<sub>3</sub>O<sub>13</sub>) was also detected in the diffractogram of this sample at 2θ equals to 30.7° (ICSD – 9378). A drop in the intensity of CeO<sub>2</sub> peaks was also observed during the reduction procedure. As the temperature reached 450 °C, it was possible to observed small peaks at 2θ equal to 26.1, 29.1, 30.0, 39.5, 46.1, 55.4 and 55.9° that could be assigned to La<sub>2</sub>O<sub>3</sub> phase (ICSD – 100204). Again, this is an indication of the perovskites phase destruction, as observed for the non-supported sample. Silvestre-Albero et al. (2002) reported the same result on their work and attributed this behavior to the presence of silica on the support.

XRD diffractograms of LaNi/AL sample (Figure 3.1C) at room temperature showed that an unexpected phase of LaNi<sub>0.5</sub>Al<sub>0.5</sub>O<sub>3</sub> (2θ equals to 23.3, 33.2, 40.9, 47.7, 53.7 and 59.3° (ICSD – 79861)) was formed and LaNiO<sub>3</sub> was also not detected. That could have occurred due to a partial insertion of aluminum from the support (Al<sub>2</sub>O<sub>3</sub>) in the perovskite structure. The formation of this phase has granted a higher thermal stability to the precursor structure, since the perovskite phase LaNi<sub>0.5</sub>Al<sub>0.5</sub>O<sub>3</sub> remained the same after the reduction process, even though it was exposed to a reductive atmosphere at 700 °C during 2 h. Thus, the presence of characteristic Ni<sup>0</sup> peaks in the reduced diffractogram of LaNi/AL can be explained by the reduction of NiO and not by the destruction of the perovskite structure. Besides, NiAl<sub>2</sub>O<sub>4</sub> phase (2θ = 37.0, ICSD – 9555) was also detected in the diffractogram of the calcined LaNi/AL, probably due to an interaction between nickel and aluminum during the synthesis process. This NiAl<sub>2</sub>O<sub>4</sub> phase probably suffered from a partial reduction, which also contributed to the formation of characteristic Ni<sup>0</sup> peaks detected at the end of the reduction period. Zhou et al. (2015) reported that when NiAl<sub>2</sub>O<sub>4</sub> spinel is exposed to temperatures between 600 and 800 °C, under a reductive atmosphere, the superficial Ni on the structure would suffer a reduction process.



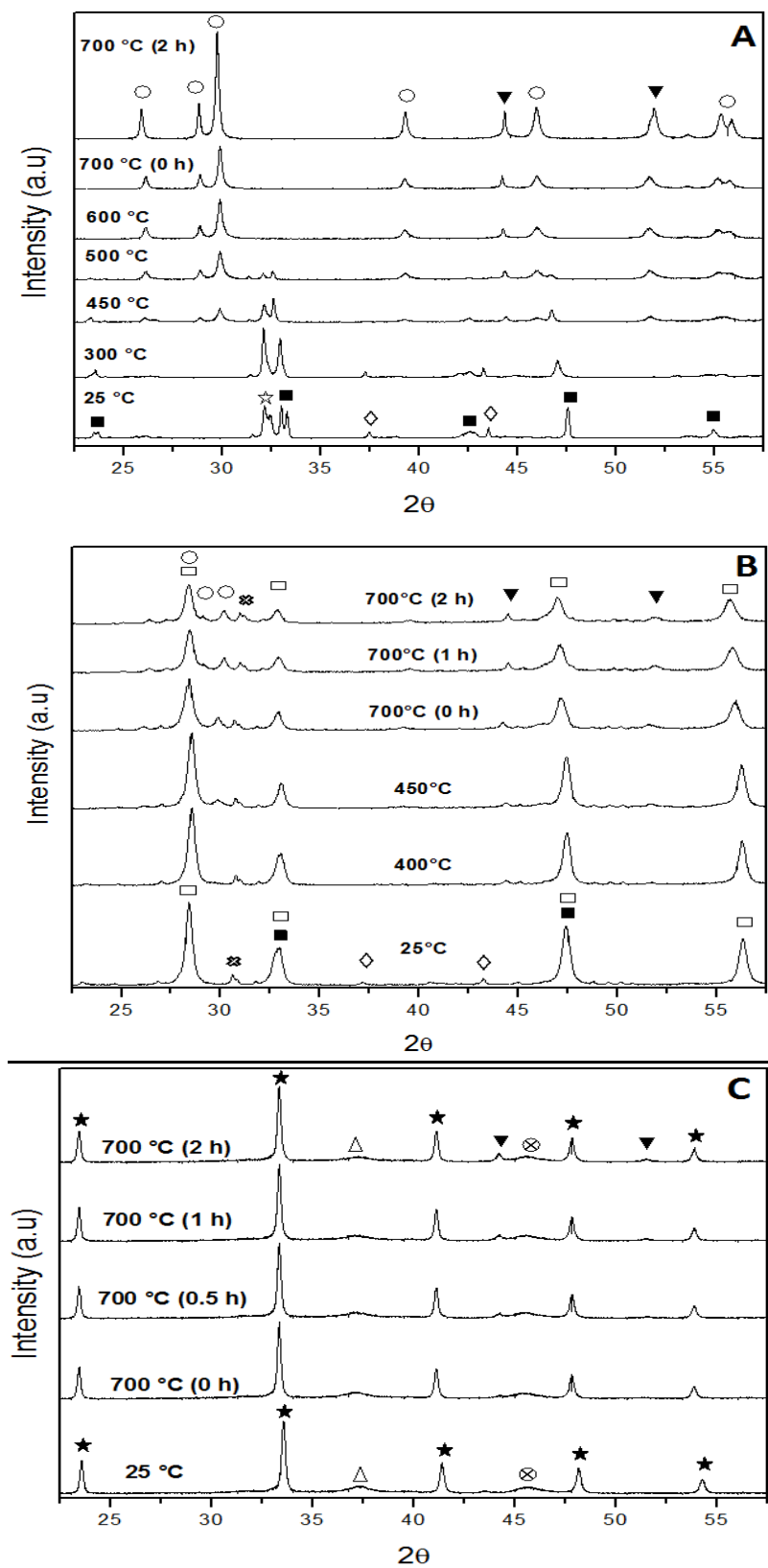


**Figure 3.1:** *in situ* XRD diffractograms of perovskite derived precursors: (A) LaNi; (B) LaNi/CS; (C) LaNi/AL. ( $\blacksquare$ ) LaNiO<sub>3</sub>, ( $\circ$ ) La<sub>2</sub>O<sub>3</sub>, ( $\diamond$ ) NiO, ( $\blacktriangledown$ ) Ni<sup>0</sup>, ( $\star$ ) La<sub>4</sub>Ni<sub>3</sub>O<sub>10</sub>, ( $\star$ ) LaNi<sub>0.5</sub>Al<sub>0.5</sub>O<sub>3</sub>, ( $\otimes$ ) Al<sub>2</sub>O<sub>3</sub>, ( $\triangle$ ) NiAl<sub>2</sub>O<sub>4</sub>, ( $\boxtimes$ ) Ce<sub>4.67</sub>Si<sub>3</sub>O<sub>13</sub> and ( $\square$ ) CeO<sub>2</sub>.

*In situ* diffractograms of the samples in different moments of the reduction process were used to evaluate Ni particle's size increase and the results were reported in Table 3.2. The analysis was conducted from when temperature immediately reached 700 °C (0 h) until the end of the reduction procedure, because at temperatures below 700 °C the Ni<sup>0</sup> characteristic peaks were still not evident, especially for LaNi/AL. It was possible to observe there was a slight growth on the average crystallite sizes of the samples, especially on LaNi which went from 17 to 23 nm. Rabelo-Neto et al. (2018) reported similar particle's size for their supported perovskite precursors reduced at temperatures around 700 °C.

**Table 3.2:** Average Ni<sup>0</sup> crystallite size growth during the reduction of the supported perovskite precursors at 700 °C.

Samples / Temperature (°C)	Ni <sup>0</sup> diameter (nm)		
	LaNi	LaNi/CS	LaNi/AL
700 (0 h)	17	13	-
700 (0.5 h)	18	14	20
700 (1 h)	20	15	21
700 (2 h)	23	15	22

XANES spectra at the Ni K-edge during the reduction under 5%H<sub>2</sub>/He mixture of the perovskite-derived precursors are shown in Fig. 3.2. At room temperature (30 °C) Ni<sup>3+</sup> oxidation state has a major contribution to the collected spectra shown in Fig. 3.2. However it is possible to affirm that there is also some contribution of Ni<sup>2+</sup> oxidation state since it was noticed the presence of NiO during the *in situ* XRD. Thus, the drop on the white line (around 8350 eV) observed for LaNi and LaNi/CS when the temperature is increased might be attributed to the reduction of both Ni<sup>3+</sup> and Ni<sup>2+</sup> to Ni<sup>0</sup>. When temperature immediately reaches 700 °C, the spectra of samples LaNi and LaNi/CS seem completely reduced, which is confirmed since Ni<sup>0</sup> oxidation state was maintained after keeping those samples during 2 h at the same temperature.

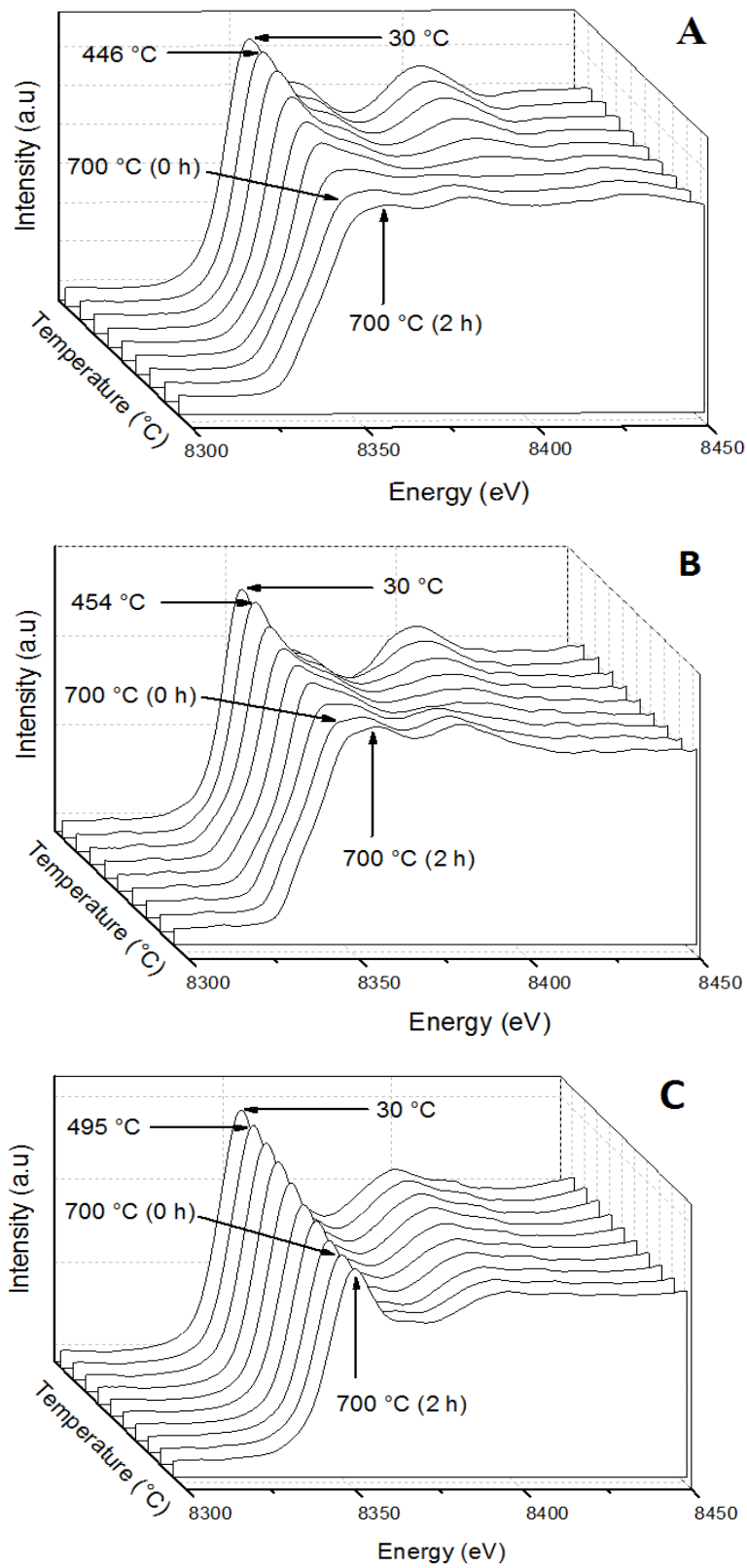


**Figure 3.2:** XANES spectra at the Ni K-edge during the reduction under 5%H<sub>2</sub>/He mixture of the perovskite-derived precursors: (A) LaNi; (B) LaNi/CS; (C) LaNi/AL.

Similar results were reported by Ávila-Neto et al. (2018) for their perovskite precursors ( $\text{LaNi}_x\text{Co}_{1-x}\text{O}_3$ ). The spectra of LaNi/AL sample (Figure 3.2 C) did not exhibit a considerable variation in the intensity of the white line, probably because most of Ni atoms remain in the perovskite  $\text{LaNi}_{0.5}\text{Al}_{0.5}\text{O}_3$  phase that was not destroyed during the reduction process due to its high thermal stability. Therefore, the majority of Ni particles did not change their oxidation state in the structure, remaining  $\text{Ni}^{3+}$ . Furthermore, one can affirm that only the small amount of Ni that stood out of the perovskite structure in the form of NiO was reduced from  $\text{Ni}^{2+}$  to  $\text{Ni}^0$  and had a little contribution on the variation of the white line, previously mentioned.

Fig. 3.3 shows the XANES spectra at  $L_{\text{III}}$  Ce-edge for sample LaNi/CS. The spectrum of the calcined sample reveals the characteristic peaks of  $\text{Ce}^{4+}$  at 5730 eV and 5740 eV, corresponding to both electronic configurations of Ce  $4f^0$  and  $4f^1$ , respectively. Increasing the reduction temperature up to 450 °C did not change the spectra, indicating that Ce remains as  $\text{Ce}^{4+}$  species. Further increase in the temperature led to a small decrease on the 5740 eV peak and a slight increase and shift on the 5730 eV peak towards 5728 eV, which is the corresponding  $\text{Ce}^{3+}$  peak, suggesting that part of  $\text{Ce}^{4+}$  is being reduced to  $\text{Ce}^{3+}$ .

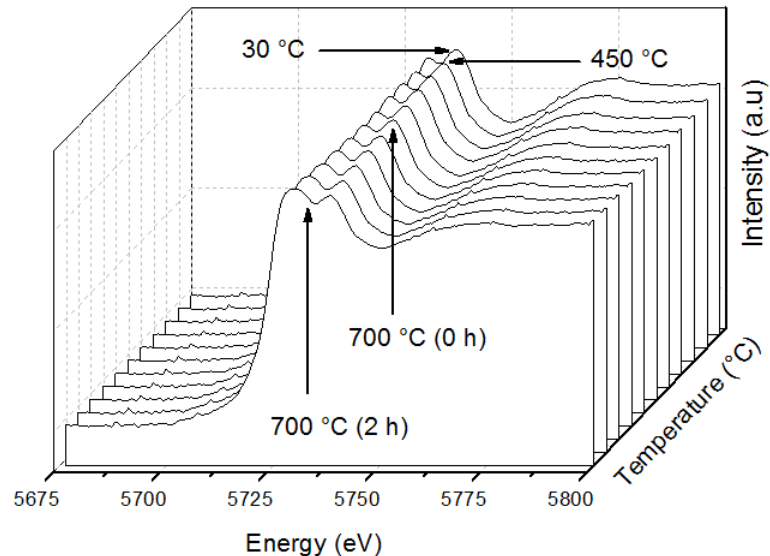


**Figure 3.3:** XANES spectra at the Ce  $L_{\text{III}}$ -edge during the reduction under 5% $\text{H}_2$ /He mixture treatment during the reduction of perovskite derived precursor LaNi/CS.

Therefore, one might affirm that those signals correspond to a mixture of  $\text{Ce}^{4+}$  and  $\text{Ce}^{3+}$  oxidative states, even though the two white lines were still noted after the exposure of LaNi/CS to a reductive atmosphere at 700 °C during 2 h. This behavior is related to the superficial reduction of ceria. Jacobs

et al. (2007) reported that the surface reduction of ceria on their Pt/CeLaAl catalysts took place at 250 °C, during the TPR-XANES analysis. However, the authors attributed the lower temperature surface reduction to the effect of promoting Pt over CeO<sub>2</sub>, which facilitated the reduction steps.

### 3.3.2. Stability Tests – Steam Reforming of LPG

Figs. 3.4 and 3.5 show the LPG conversion and the dry molar fraction of the studied species at 600 °C as a function of time-on-stream (TOS) for the SRLPG over the perovskite-derived catalysts.

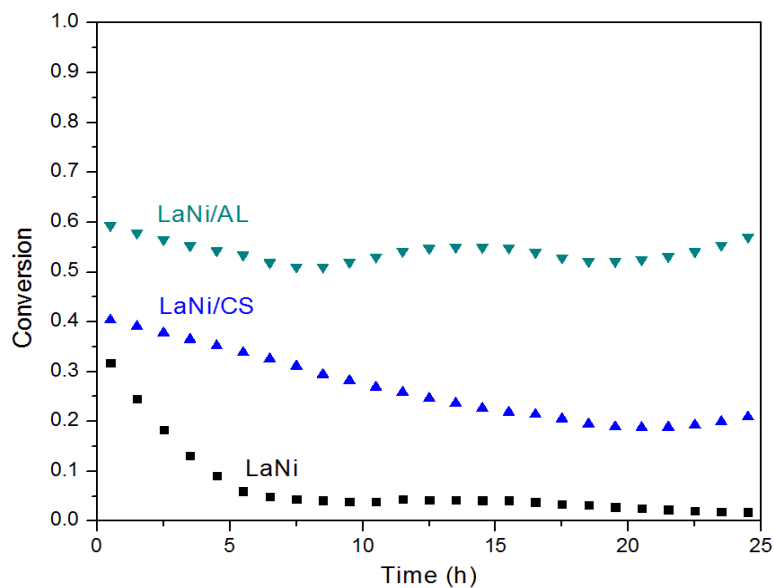


**Figure 3.4:** LPG conversions during the SRLPG at 600 °C over the perovskite-derived catalysts, using a GHSV of 1200 L/g<sub>Ni</sub>·h.

LaNi catalyst exhibited a strong deactivation during the first 5 h of TOS and did not have any significant activity after 25 h of TOS. Silva et al. (2017) reported similar results for their perovskite derived catalyst. The authors attributed the deactivation of their catalysts to coking, which occurred due to the low operation temperature. According to the authors the 600 °C temperature favors hydrocarbons decomposition but limits the reaction of carbon species with the oxygen from water (reverse Equation 3.11), causing carbon deposition on the catalyst surface.

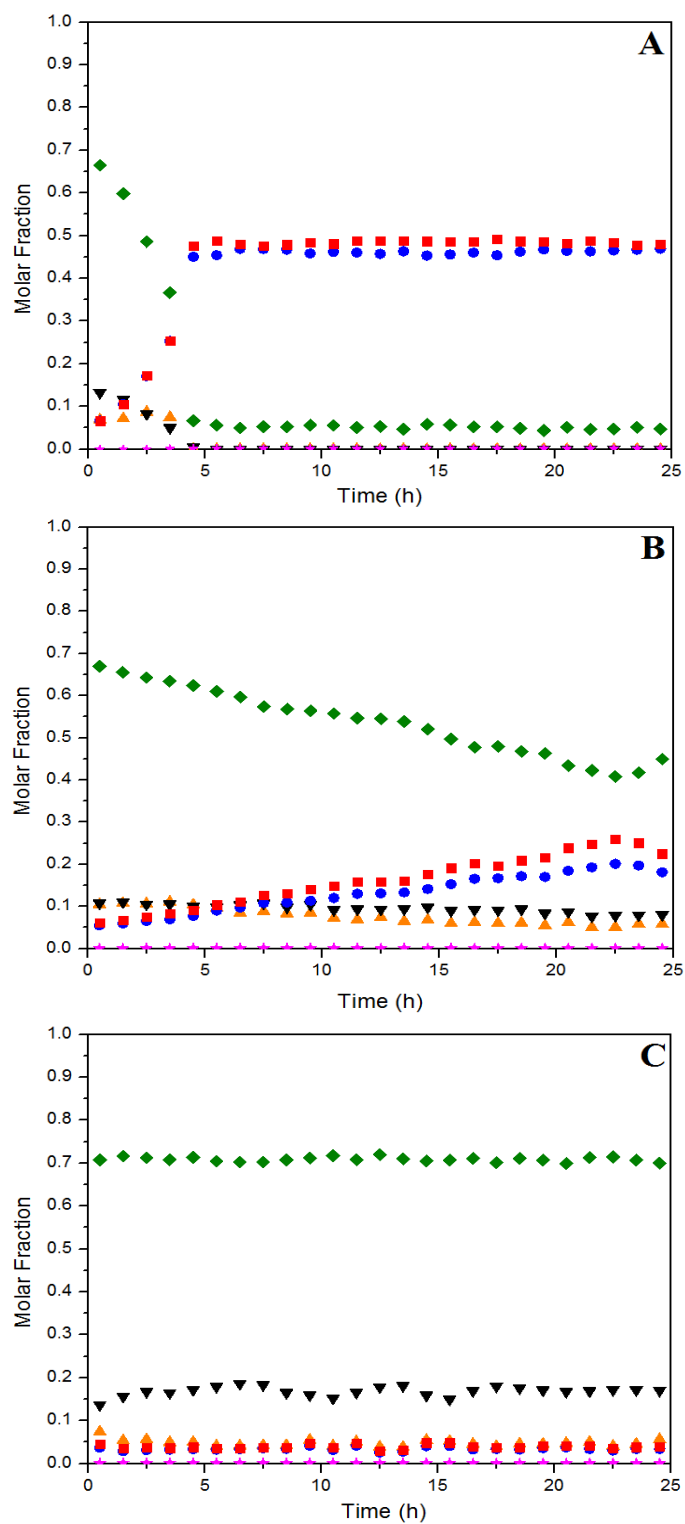


**Figure 3.5:** Species molar fraction during the SRLPG at 600 °C over the perovskite-derived catalysts. (A) LaNi; (B) LaNi/CS; and (C) LaNi/AL. (●) Propane, (■) Butane, (◆) H<sub>2</sub>, (▼) CO<sub>2</sub>, (▲) CO, (★) CH<sub>4</sub>.

The addition of supports in the perovskite-derived catalysts lead to an improvement in the catalytic performance since LaNi/CS and LaNi/AL showed considerably better activity and stability than the non-supported one. A relatively high initial LPG conversion (around 40%) was obtained by catalyst LaNi/CS, but it suffered a gradual drop reaching only 20% by the end of the test. The same behavior was observed for the hydrogen molar fraction (Figure 3.5 B) which drops from 65 to 45%. The progressive deactivation process of LaNi/CS catalyst might be ascribed to a partial oxidation of the catalyst's metallic phase due to an overall oxidative atmosphere, characteristic of steam reforming processes. Pereniguez et al. (2010) attributed the deactivation of their perovskite precursors during the steam reforming of methane to the gradual oxidation of Ni phase. According to the authors, even though the derived-perovskite precursors were tested under steam and dry reforming of methane, the loss of activity occurred only on the former process due to the oxidative conditions of the reaction. Moreover, no considerable deposits of solid carbon were observed after their SRM reaction, which reinforces the author's hypothesis. It is not likely that part of the deactivation observed on LaNi/CS was due to coking. The well-known oxygen mobility of ceria supports promotes carbon gasification on the catalyst, which considerably diminishes the amount of carbon deposits over the active Ni sites. The redox mechanism and the oxygen mobility of ceria compounds and their advantages when used with Ni catalysts are well documented in the literature (Laosiripojana and Assabumrungrat, 2006; Laosiripojana and Assabumrungrat, 2005; Huang et al., 2005; Reddy and Khan, 2005).

Among the supported catalysts, LaNi/AL had the highest LPG conversion that oscillated around 55% during the reaction period. The better performance of this sample might not only be related to its higher surface area but also to a possible partial reduction of the  $\text{NiAl}_2\text{O}_4$  phase. Chen and Ren (1994) studied the dry reforming of methane using a series of Ni/ $\text{Al}_2\text{O}_3$  catalysts calcined at different temperatures. Their results showed that  $\text{NiAl}_2\text{O}_4$  phase was not active for methane dry reforming. However, they pointed out that the reduced form of  $\text{NiAl}_2\text{O}_4$  could lead to significant increase in activity and stability in this reaction. Hence, it is deduced that the higher activity of Ni/g- $\text{Al}_2\text{O}_3$  in this investigation was probably due to the synergetic effect of the reduced  $\text{NiAl}_2\text{O}_4$  and surface nickel particles. More recently, Zhou et al. (2015) investigated the effect of  $\text{NiAl}_2\text{O}_4$  on the stability of Ni/ $\text{Al}_2\text{O}_3$  catalysts for dry reforming of methane. The authors showed that using reduction temperatures between 600 and 800 °C leads to a surface reduction of the  $\text{NiAl}_2\text{O}_4$  spinel structure. According to them, the incomplete reduction of this phase generates more Ni sites with strong interaction with the support, which contributes to a better stabilization of the particles and consequently increases the catalyst activity.

It was possible to observe through Fig. 3.5 C that LaNi/AL presented molar fractions of carbon products close to the ones of LaNi/CS. While the former showed around 15% of CO<sub>2</sub> and 5% of CO, the latter produced around 10% of both CO and CO<sub>2</sub>. The higher conversion and the resembling molar fraction of carbon products between the two samples might be an indication that decomposition reactions, such as the ones described in Equations 4.9 to 4.14, are occurring in LaNi/AL. Therefore, it is expected a high carbon formation for this catalyst.

The amount of hydrogen produced during the stability tests of the SRLPG was also analyzed. Average hydrogen yields were estimated in three different periods of the reaction as listed in Table 3.3. LaNi/AL showed the highest hydrogen yield among all catalysts, which remained constant during the reaction. This behavior was expected since this sample had the highest average LPG conversion and hydrogen molar fraction during the stability tests. LaNi/CS presented the second highest hydrogen yield followed by LaNi. Furthermore, the hydrogen yield gradually decreased as the LaNi/CS catalyst deactivated during TOS.

**Table 3.3:** Estimated average hydrogen yield considering the fed LPG during different periods of the stability test.

Samples	Average Hydrogen Yield (mols H <sub>2</sub> /mols LPG)		
	0 to 5 h	5 to 15 h	More than 15 h
LaNi	1.41	0.06	0.05
LaNi/CS	2.68	1.60	0.91
LaNi/AL	4.23	4.58	4.39

The different performances of each catalyst are related to the reaction mechanism of SRLPG. Hibbits et al. (2016) conducted a study about the effects of n-alkanes chain length on the mechanism of metal-catalyzed hydrogenolysis. According to them, C-C bond breaking of propane and butane are the only kinetic relevant steps on the mechanism since C-H and H-H bond dissociations are considered a quasi-equilibrium state. After the C-C cleavage, CH<sub>x</sub> species shall be formed and react with the adsorbed hydrogen atoms on the surface of Ni metal producing methane. On the other hand, the formed CH<sub>x</sub> species may also decompose to carbon and hydrogen through the dehydrogenation reaction. In our work, it was noticed that methane production was close to zero while the catalysts were active to the SRLPG. Therefore, it is possible to infer that CH<sub>x</sub> species are following the decomposition route, which could explain possible carbon formation rates on LaNi and LaNi/AL catalysts during the reactions performed at 600 °C. In LaNi/CS the effect of mechanism that favors carbon deposition was probably attenuated due to the oxygen mobility of the support. When oxygen



mobility through the metal-support interface is facilitated,  $\text{CH}_x$  species can be easier oxidized into CO or  $\text{CO}_2$ . Faria et al. (2016) obtained resembling results for their Ni/Ce/Al catalysts during the SRLPG.

The SRLPG was also carried out at a higher temperature (700 °C) and the results are shown in Figs. 3.6 and 3.7.

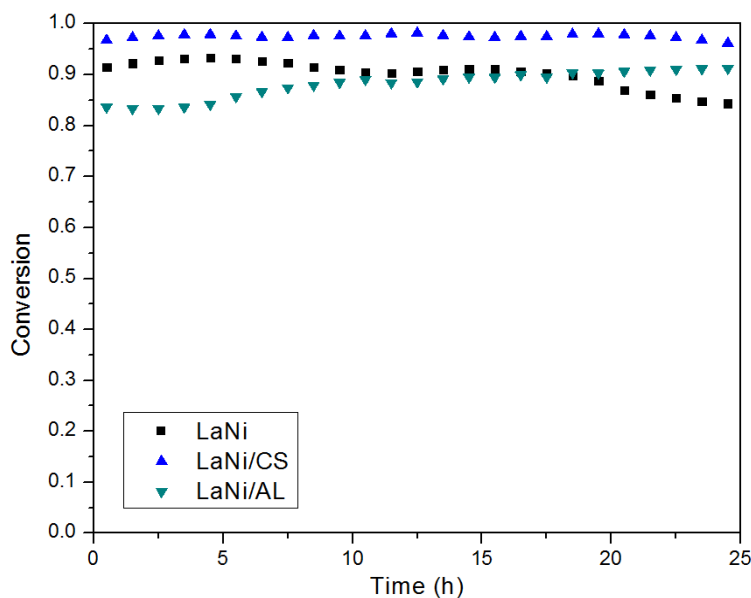


**Figure 3.6:** LPG conversion during the SRLPG at 700 °C over the perovskite-derived catalysts.

The increase in the reaction temperature leads to a higher average LPG conversion for all catalysts. LaNi/CS showed the best performance reaching almost 100% of LPG conversion. In addition, it is noticed that stability was highly improved by the temperature increase, as the conversion of the reactants remained almost the same to the initial one, even after 24 h of reaction, for all samples. Average hydrogen yield was also estimated for the reaction at 700 °C and it did not suffer a considerable variation during the 24 h test. The highest  $\text{H}_2$  yield was obtained by LaNi/CS (8.75 mols of  $\text{H}_2$ /mols of LPG). Hydrogen yields of LaNi and LaNi/AL samples were approximately 7.54 and 7.41 mols of  $\text{H}_2$ /mols of LPG, respectively. Trimm (1999) explained this effect suggesting that the main products of the steam reforming reaction of light hydrocarbons are strongly related to temperature. Methane formation is favored at lower temperatures, while hydrogen production is facilitated at higher temperatures, between 700 and 800 °C. Although it is known the latter temperature may be propitious to carbon formation due to the dehydrogenation of  $\text{CH}_x$  species mechanism, the author affirms that the reverse reaction described in Equation 3.11 ( $\text{CO} + \text{H}_2 \rightleftharpoons \text{H}_2\text{O} + \text{C}_{(s)}$ ) is favored, which helps to improve the catalysts performance and to maintain its activity.

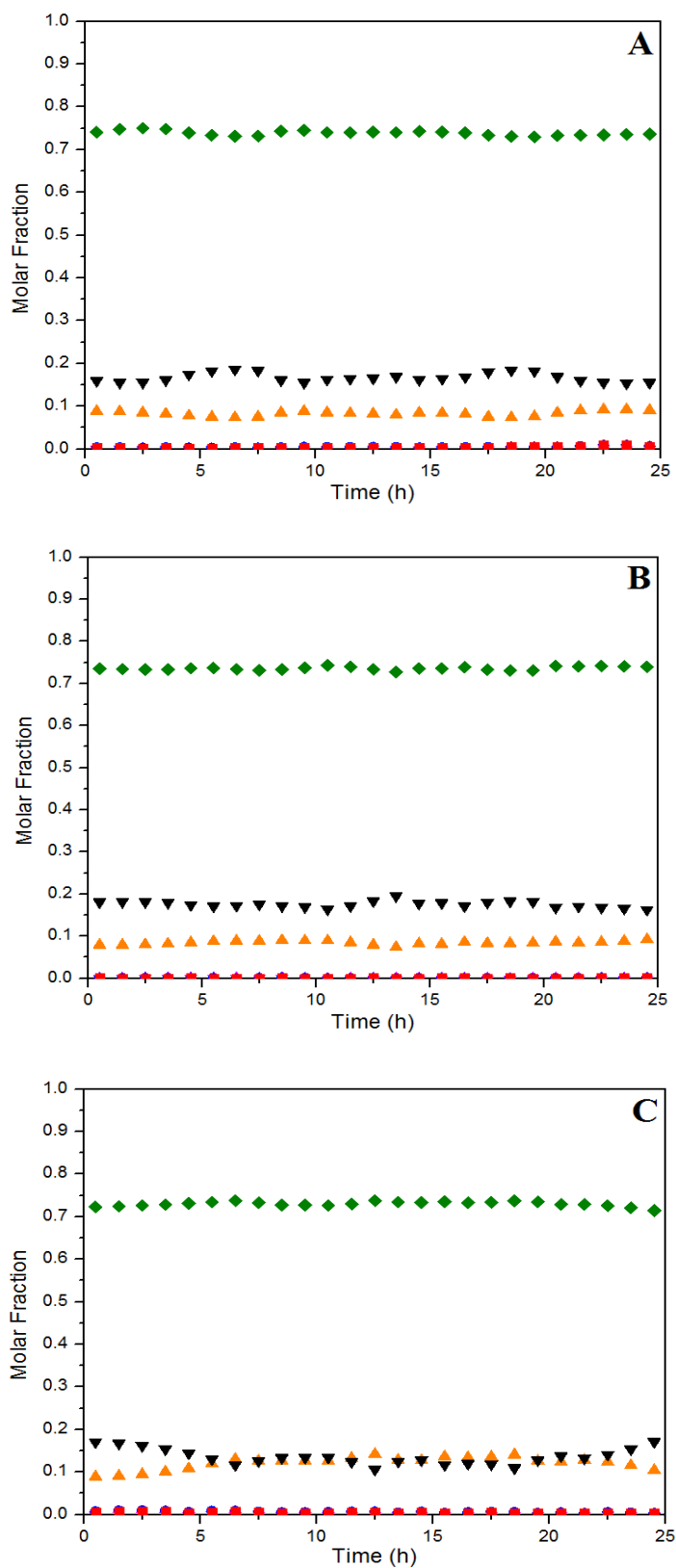


**Figure 3.7:** Species molar fraction during the SRLPG at 700°C over the perovskite-derived catalysts LaNi (A), LaNi/CS (B) and LaNi/AL (C), where (●) Propane, (■) Butane, (◆) H<sub>2</sub>, (▼) CO<sub>2</sub>, (▲) CO, (★) CH<sub>4</sub>.

Wang et al. (2009) also obtained resembling similar hydrogen yields during their thermodynamic simulations and concluded that the optimum operation condition for the steam reforming of propane is using a water/carbon molar rate between 4 and 6 and at temperatures between 650 and 700 °C.

### 3.3.3 Thermogravimetric Analysis (TGA)

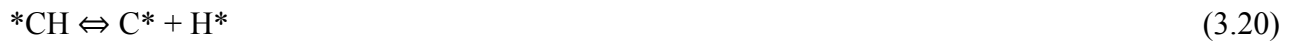
TGA analysis of the used catalysts after reaction at 600 and 700 °C was performed to measure the amount of carbon deposited. The results are reported in Table 3.4. After reaction at 600 °C, the highest carbon formation rate was observed for the unsupported catalyst. The lowest amount of carbon was detected on ceria-silica supported perovskite-derived catalysts.

**Table 3.4:** Carbon formation rate estimated by the TGA analysis of the perovskite-derived catalysts after 24 h of SRLPG reaction.

Samples	Carbon formation rate (mg C/g cat.h.g. <sub>reacted</sub> )	
	600 °C	700 °C
LaNi	3.93	0.25
LaNi/CS	0.71	0.22
LaNi/AL	3.41	0.23

Fig. 3.4 shows significant deactivation of the LaNi catalyst, which could be attributed to significant carbon deposition. Similar results were reported by Silva et al. (2017), in which high coking rates were attributed to relatively low reaction temperature, consistent with the results here. Literature shows that the characteristic acid sites of alumina support can favor undesired decomposition reactions, like the ones seen in Eqs. 3.4-3.14, which promotes coke deposition over the catalyst (Wang and Lu, 1998). However, although LaNi/AL presented slightly lower carbon deposition rates than LaNi, LaNi/AL did not suffer from deactivation by coking (Fig. 3.4). Zhou et al. (2015) attributed a similar behavior of their catalysts to the partial reduction of NiAl<sub>2</sub>O<sub>4</sub> spinel and a strong interaction between the metallic phase and the support. According to the authors, the Ni support interaction may form a defective Ni<sub>x</sub>Al<sub>y</sub>O<sub>z</sub> phase, which might present a higher oxygen surface mobility favoring a faster rate of carbon gasification. Furthermore, the strong metal-support interaction prevents the catalysts from deactivation because it contributes to the formation of carbon nanotubes, which form an active Ni particle on the top of the tubes. LaNi/CS found a much lower carbon accumulation rate at 600 °C than either of the other catalysts. The well-known oxygen mobility of ceria and the redox properties of ceria-based materials appear to significantly contribute

to the removal of carbon mechanism. If so, this is the result of the reaction between the formed solid carbon and the active oxygen species provided by the support resulting in gasified products, CO and/or CO<sub>2</sub>. When the SRLPG reaction was carried out at 700 °C, all catalysts exhibited much lower carbon accumulation rates. The same effect was observed by Zanchet et al. (2015) while studying ethanol reforming. The authors reported that at high temperatures such as the one used in the last stability tests (700 °C) favor the activation of steam in reforming reactions (Eqs. 3.18 and 3.19). Steam activation is essential in the oxidative process of CH<sub>x</sub> species since the decomposed C\* reacts with O\* species provided by water dissociation. Thus, this mechanism minimizes carbon deposition on the catalyst surface and avoids the blockage of the active sites, which allows a longer catalytic activity. The CH<sub>x</sub> species oxidation mechanism was also reported by Zanchet et al. (2015) and it is described through Equations 3.20-3.22.



According to the literature, carbon accumulation on the catalyst surface may happen due to a combination of different mechanisms such as hydrocarbon decomposition, Boudouard reaction, and polymerization reactions (Alberton et al., 2007; Basagiannis and Verykios, 2006). Thermodynamic studies have shown that the increase in reaction temperature disfavors carbon deposition, for different hydrocarbons reforming processes (Alberton et al., 2007; Basagiannis and Verykios, 2006). Both hydrocarbon decomposition and Boudouard reactions are thermodynamically disfavored at higher temperatures. On the other hand, the rates of the reactions that gasify carbon, such as the inverse of Boudouard reaction (3.10), increase with temperature. For instance, Basagiannis and Verykios (2006) reported the carbon deposition as a percentage of the carbon fed to the reactor during the steam reforming of acetic acid. When they used a Ni/La<sub>2</sub>O<sub>3</sub>/Al<sub>2</sub>O<sub>3</sub> catalyst, at 500 °C, 6.7% of the carbon fed was deposited on the surface. When the reaction temperature was increased to 700 °C, this value was reduced to 0.43%. The same type of trend was observed by Alberton et al. (2007) in investigations about the steam reforming of ethanol. In this study, the researchers measured the weight loss during thermogravimetric analysis after the steam reform of ethanol using

an 8%Ni/Al<sub>2</sub>O<sub>3</sub> sample. The weight loss was 45% at 500 °C, 25% at 600 °C, and 20% at 700 °C. More recently, Ferreira et al. (2019) studied hydrotalcite type precursors for the steam reforming of LPG in the same conditions used in this work. They reported a carbon deposition rate of 31.4 mgC/gcat.h for the reaction at 600 °C. However, at higher temperatures (700 and 800 °C) this rate dropped to values around 4 mg C/gcat.h.

### 3.4. Conclusions

This work evaluated the influence of supporting perovskite-type precursors during the steam reforming of LPG, using propane and butane as model molecules. XRD characterization showed the presence of NiO phase in all precursors which suggests that part of nickel was outside of the perovskite structure. *In situ* XRD and *in situ* XANES on nickel K-edge indicated that all precursors were reduced after exposed to 700 °C during 2 h, destroying the perovskite type structure. The only exception was LaNi/AL, which presented a higher thermal stability due to the formation of LaNi<sub>0.5</sub>Al<sub>0.5</sub>O<sub>3</sub> and NiAl<sub>2</sub>O<sub>4</sub> phases. *In situ* XANES on cerium L<sub>III</sub>-edge analysis showed the superficial reduction of ceria and also indicated a possible interaction between Ni metallic sites with the support. There was a significant contribution of the supports in the catalytic activity during the SRLPG at 600 °C because both supported perovskites presented higher conversion and stability than the non-supported one. LaNi/CS showed a gradual deactivation probably because of a metallic phase oxidation. The catalyst also had a low carbon accumulation rate due to the oxygen mobility of the support that helps the gasification of solid carbon on catalyst surface. LaNi/AL remained active during the whole analysis especially due to the strong Ni-support interaction provided by the partial reduction of NiAl<sub>2</sub>O<sub>4</sub>, which contributes to carbon nanotubes formation and avoids the blocking of Ni sites. Temperature had a major role on the catalysts activity as they could reach conversions from 80 to 100% on 700 °C stability tests. When temperature was increased to 700 °C, carbon accumulation was negligible for all catalysts, since this condition favors the mechanism of water activation and consequently avoids carbon deposition through the oxidation process of CH<sub>x</sub> species into CO and CO<sub>2</sub>.

### ACKNOWLEDGMENTS

The authors wish to acknowledge the financial support of CAPES, FAPEMIG and CNPq. We also thank LNLS for the use of XPD and DXAS beamlines.

## **CHAPTER 4 - HYDROGEN PRODUCTION FROM THE STEAM REFORMING OF PROPANE USING SUPPORTED NICKEL OVER CERIA-SILICA CATALYSTS.**

ABSTRACT – The effect of silica molar content on the performance of Ni/CeO<sub>2</sub>-SiO<sub>2</sub> during the steam reforming of propane was investigated. Nickel precursors supported over ceria-silica with different molar contents of ceria:silica (65:35%, 75:25%, 85:15% and 100:0%) were synthesized and named Ni65CS, Ni75CS, Ni85CS and NiCe, respectively. BET surface area and *in situ* XRD results showed that a higher silica molar content in the support contributes to an increase in the surface area and to smaller Ni average crystallite size. Temperature Programmed Reduction and *in situ* X-ray absorption near edge spectroscopy indicate a direct relationship between the silica molar content on the metal-support interaction and ceria dispersion and reducibility. Ni65CS and Ni75CS had lower carbon accumulation rate than the other catalysts, as demonstrated by thermogravimetric analysis. Ni75CS presented the highest conversion (around 75%) during catalytic tests at 600 °C and did not suffer from deactivation after 25 h. Based on the results, the optimum ceria:silica content in the support was 75:25%, since this produced a more stable catalyst and smaller carbon deposition.

Keywords: Propane, Ceria-silica, Hydrogen.

## 4.1. Introduction

The study of hydrogen production has been increasing in recent years as a consequence of a growing demand for efficient, clean and sustainable fuels by global community. Although hydrogen can be produced by renewable feedstock like biomass and water, these processes are not economically attractive nowadays (LeValley et al., 2014). Until cost-effective technologies to produce hydrogen from renewable sources are yet to be developed, fossil fuels like methane, naphtha and liquefied petroleum gas (LPG) can be used to obtain this gas by steam reforming processes in a transition scenario from non-renewable to renewable feedstock (Izquierdo et al., 2012).

Ni-based catalysts are commonly chosen for steam reforming processes since they have long-proven satisfactory performance and a considerably lower cost when compared to noble metals like Pt, Pd, Rh and Ru (Zhang et al., 2009). However, it is well known that they suffer from deactivation by coke deposition especially when higher hydrocarbons are reformed at relative low steam/carbon ratio (Natesakhawat et al., 2005).

A plausible alternative in the attempt to avoid carbon deposition on Ni catalyst is the use of promoters. There are plenty reports in literature relating that lanthanides can act as good promoters for nickel-based catalysts since they are able to inhibit carbon deposition without interfering on catalytic activity. Amin et al. (2015), investigated the doping effect of Pr, Nd, Sm, Eu, Gd, Tb, Dy, Ho, Er, and Tm on the activity of Ni catalysts during the dry reforming of methane. The results showed that promoted Ni catalysts exhibited a considerably high stability since they kept active when the reaction was performed up to 60 h. The authors ascribed the better stability of the promoted catalysts as a consequence of low amounts of carbon deposition compared with unpromoted catalyst. Natesakhawat et al. (2005) studied the effect of La, Ce and Yb on Ni/Al<sub>2</sub>O<sub>3</sub> catalysts during the steam reforming of propane. In their work the authors noticed a beneficial role of the lanthanide elements on the catalytic activity and stability since they were able to enhance catalyst reducibility and resistance to deactivation. It was also reported that the positive effect is more evident with cerium addition due to its higher conversion and hydrogen yield, especially when the reaction was conducted at 550 °C.

Ceria-based supports are widely used for a variety of hydrocarbon reactions to produce hydrogen. These materials have some desirable characteristics that make their use in steam reforming systems more attractive, such as their high oxygen storage capacity and oxygen mobility which favor carbon removal mechanism and increase catalyst stability. The strong interaction with the metallic phase of the system (metal-support interaction) also helps the stabilization of the catalyst. Moreover, ceria ability to fast interchange between Ce<sup>4+</sup> and Ce<sup>3+</sup> improves the reactions

rates of carbon species and its lattice oxygen (Liu et al., 2011; Laosiripojana et al., 2011). However, ceria-based materials still suffer from the loss of surface area when exposed to high temperatures, as the ones normally used on steam reforming processes. Temperature increase lead to sintering phenomena on ceria particles which is one of the main causes to catalyst deactivation (Rocchini et al., 2000).

In order to grant higher thermal stability to ceria-based materials and to enhance its surface area some promoters like silica ( $\text{SiO}_2$ ) might be associated with them and be used as mixed oxides supports. Rocchini et al. (2002) explained that ceria-silica promotion is related to a new phase/compound formation that is responsible to induce small ceria crystallite stabilization and decreases the reduction temperature of the material. When the promoted material is reoxidized the previous formed phase is decomposed into amorphous silica, which is known to be effective surface-area-stabilizing agent and into small ceria crystallites, which are more susceptible to reduction processes.

There are some reports showing the improvement of nickel catalytic activity when ceria is mixed with silica. Yap et al. (2013) have studied the dry reforming of methane using 5 wt.% supported nickel catalysts on ceria-silica (CS) with different loadings of ceria ( $x = 3, 9, 18,$  and  $30$  wt.%). In their work it was observed that the  $\text{Ni}/x\text{CS}$  ceria-silica catalysts showed better performance, stability and a lower carbon formation rate than the precursors supported over pure silica or ceria ( $\text{Ni}/\text{SiO}_2$  or  $\text{Ni}/\text{CeO}_2$ ). The authors ascribed this result to the higher reducibility, basicity, metal dispersion and smaller Ni particle size of the promoted ceria-silica catalysts when compared to the non-promoted ones. Zhao et al. (2017) reported the performance of encapsulated  $\text{Ni}/\text{CeO}_2\text{-ZrO}_2$  by silica during the steam reforming of toluene and found that the addition of silica contributed on higher catalytic activity. Under  $650$  and  $700$  °C temperatures the most active catalyst reached 60% and 80% of toluene conversion, respectively. According to the authors the better performance of promoted ceria-zirconia-silica catalysts is related to enhanced Ni activity due to the partial oxidation of Ni atoms at  $\text{Ni-SiO}_2$  interface.

In the previous chapter we have shown the benefits of supporting a perovskite precursor over ceria-silica during the steam reforming of LPG, as the catalyst presented a low carbon deposition amount even after 24 h of reaction. This result could be attributed to the high oxygen storage capacity and redox properties of ceria-based materials which allows them to gasify the deposited carbon over the catalyst surface into CO and  $\text{CO}_2$ .

In this work we investigated the effect of the molar variation of silica over ceria on the catalytic activity during the steam reforming of propane, used as a model molecule of LPG.



## 4.2. Methodology

### 4.2.1. Catalyst preparation

Four Ni catalysts supported over ceria-silica 10%wt Ni/xCeO<sub>2</sub>-(1-x)SiO<sub>2</sub> (x = 0.65, 0.75, 0.85 and 1.00) were prepared by wet impregnation in this work. They were named Ni65CS, Ni75CS, Ni85CS and NiCe, respectively. Mixed oxides CeO<sub>2</sub>-SiO<sub>2</sub> supports were previously prepared by coprecipitation method using (NH<sub>4</sub>)<sub>2</sub>Ce(NO<sub>3</sub>)<sub>6</sub> (Aldrich) and SiO<sub>2</sub> (Aerosil 380) as reactants. A NH<sub>4</sub>OH solution (1 mol/L) was continuously added dropwise to the solution of Ce(IV) nitrate during 30 min under constant stirring at room temperature. SiO<sub>2</sub> (Aerosil 380) was solubilized using a KOH alkaline solution (1 mol/L) under constant stirring at 100 °C. Afterwards, the boiling silica alkaline solution was added to the ceria suspension under constant stirring at room temperature and aged for another 30 min. Then, the final suspension was washed and vacuum filtered several times with distilled water until the effluent pH became neutral (pH = 7.0 ± 0.5). A yellow precipitate was formed and dried at 110 °C during 12 h and macerated into a fine powder. A nickel nitrate aqueous solution was added on the four supports by the wet impregnation method. Finally, each impregnated support was calcined from room temperature to 500 °C with a temperature ramp rate of 5 °C/min under an air flow of 50 mL/min, during 4 h.

### 4.2.2. Characterization

#### 4.2.2.1. CO<sub>2</sub>-TPD

CO<sub>2</sub>-TPD experiments were conducted using 35 mg of each sample and measured in the Louisiana State University facilities using a thermal conductivity detector (Altamira AMI-200). The samples were dried at 110 °C during 30 min under a 30 mL/min He flow. Then, they were saturated with carbon dioxide at 50 °C under a 10% CO<sub>2</sub>/He stream for 30 min. Afterwards, physisorbed CO<sub>2</sub> was purged using a 30 mL/min He flow for 30 min and, finally, CO<sub>2</sub> desorption was conducted under He flow (30 mL/min) increasing the temperature from 50 °C to 900 °C at 10 °C/min.

#### 4.2.2.2. BET Area

BET surface areas of the samples were measured in the Louisiana State University facilities using a thermal conductivity detector (Altamira AMI-200) by nitrogen adsorption at – 190 °C. Before the analysis, all samples were dried in Helium flow at 150 °C, for 30 min.

#### 4.2.2.3. *In situ X-Ray Diffraction (in situ XRD)*

*In situ* XRD characterization test was done using a CuK $\alpha$  radiation of 1.5498 Å and an energy of 8 keV in a diffractometer (Huber) in D10B-XPD beamline of LNLS in Campinas-BRAZIL. Samples were monitored in a  $2\theta$  range from 22 to 58°, with 0.003° step and 1 s of counting time, while they were exposed to a reducing atmosphere of 5% H<sub>2</sub>:He (100 mL/min). During the procedure, temperature was increased with a heating rate of 10 °C/min from 25 to 500 °C and kept in 500 °C for 1 h. After the reduction process, Scherrer equation was used to estimate Ni<sup>0</sup> average crystallite sizes.

#### 4.2.2.4. *Temperature Programmed Reduction (TPR)*

TPR measurements were performed in the Louisiana State University facilities with a thermal conductivity detector (Altamira AMI-200). It was used 20 mg of each the ceria-silica supported Ni precursor in a quartz reactor, where they were heated from room temperature to 1000 °C, at a 10 °C/min heating rate, under 30 mL/min flow of a 10% H<sub>2</sub>:Ar mixture.

#### 4.2.2.5. *X-Ray Absorption Near Edge Structure (XANES)*

XANES characterization test was conducted at DXAS beamline at LNLS (National Laboratory of Synchrotron Light) in Campinas - BRAZIL. Precursors and boron nitrate were mixed considering an optimum weight to maximize the signal-to-noise ratio in the ionization chambers and used to prepare pellet samples. All samples were monitored in nickel K-edge (8333 eV) and cerium L<sub>III</sub>-edge (5723 eV) during both a reduction and a reaction process. During the reduction procedure a 5% H<sub>2</sub>:He (100 mL/min) mixture was used and the temperature was raised, with a heating rate of 10 °C/min, from 25 to 500 °C and kept at 500 °C for 1 h. After reduction, temperature was increased from 500 to 600 °C in order to start the steam reforming of propane process. The reaction was performed during 1 h, using as reactants a mixture of 20% Propane:He and water, which was fed through a saturator. Propane/steam molar proportion was kept in 1/6. Software ATHENA/IFEFFIT was used to treat XANES data. A normalization procedure was done subtracting a straight line from the pre-edge border and multiplying the corresponding spectrum in all analyzed data in order to guarantee that spectra oscillations would happen around a normalized axis.

#### 4.2.3.1 Catalytic Performance

Stability tests were evaluated at 600 °C, during 24 h, using fixed bed reactor. 10 mg of precursors were mixed with 50 mg of quartz, used as an inert. The mixture of precursor and inert was charged into a quartz tube reactor and reduced with a pure H<sub>2</sub> flow of 30 mL/min at 500 °C for 1 h. Propane was used as a model molecule of LPG and it was fed into the reactor at a 20 mL/min flow rate. Water feed was set considering a steam to carbon molar ratio of 2, i.e., S/C = 2. Liquid water was continuously pumped into heated lines where it was vaporized at 150 °C and carried to the reactor with a Helium flow of 30 mL/min. The effluent gases were analyzed using gas chromatography (GC-2014, SHIMADZU) with TCD (column Carboxen 1010) and FID (column Rt-QPLOT) detectors. Propane conversion ( $X_{C3}$ ) and the selectivity of products ( $S_{i \text{ product}}$ ) were calculated according to the following equations:

$$X_{C3} = \frac{F_{C3}^{in} - F_{C3}^{out}}{F_{C3}^{in}} \quad (4.1)$$

$$S_i = \frac{F_i}{\sum F_i} \quad (4.2)$$

Where “F” is the molar flow rate and “i” corresponds to species of the reactor’s inlet or outlet.

The steam reforming of propane reaction was also conducted at 400 °C for 1.5 h in order to guarantee a kinetic condition regime and thus, to evaluate each catalysts performance. The collected data was used to estimate the reaction rate of each precursors, which can be described according to the following equation:

$$R_p = \frac{n_{P(reac)}}{(m_{cat} \cdot t)} \quad (4.3)$$

Where  $n_{P(reac)}$  corresponds to the number of mols converted during the reaction,  $m_{cat}$  (g) is the mass of catalysts used in the analysis and  $t$  (h) corresponds to the TOS.

#### 4.2.3.2 Thermo Gravimetric Analysis (TGA)

TGA was performed to quantify carbon deposition in the derived perovskite-type precursors. The analysis was done using a SDT Q600 (TA instrument) linked to a thermo-balance. All samples were heated from room temperature to 1000 °C in air atmosphere, using a 10 °C/min heating rate. Through the TGA results, a carbon formation rate ( $R_C$ ) was estimated dividing the mass of solid carbon ( $mgC_{(s)}$ ) by the used catalyst mass ( $g_{Cat}$ ), reaction time ( $t$ ) and the mass of reacted carbon ( $mgC_{react}$ ) in each stability test. The main goal of considering the last parameter is to measure how much of the reacted carbon turned into coke and so to establish a fairer comparison between the catalytic systems.

$$R_C = \frac{mgC_{(s)}}{(g_{cat}.t.mgC_{react})} \quad (4.4)$$

## 4.3 Results and Discussion

### 4.3.1 Catalysts Characterization

*In situ* XRD results of the ceria-silica supported Ni precursors Ni65CS (A), Ni75CS (B), Ni85CS (C) and NiCe (D) are reported in Figure 1. At room temperature, the expected NiO characteristic peaks at  $2\theta$  equals to  $37.2^\circ$  and  $43.3^\circ$  (ICSD: 9866) were observed for all samples. After the samples were exposed to  $500^\circ\text{C}$  during 60 min in reducing atmosphere, NiO phase was replaced by characteristic Ni<sup>0</sup> peaks which can be seen at  $2\theta$  equals to  $44.1$  and  $51.8^\circ$  (ICSD – 260169). At room temperature, cerium oxide (CeO<sub>2</sub>) characteristic peaks were also observed at  $2\theta = 28.6, 33.1, 47.5$  and  $56.4^\circ$ . Das et al. (2018) reported the same peaks for their ceria-silica supported precursors. *In situ* XRD results indicated that the addition of silica in the support contributed to diminish the sintering effect on ceria particles, since precursors with a higher content of SiO<sub>2</sub>, i.e. Ni65CS (A) and Ni75CS (B), presented broad and less intense ceria peaks, while Ni85CS (C) and NiCe (D) that have a lower silica content presented sharper and more intense ceria peaks. A similar effect was observed for the metallic nickel phase as larger and less intense Ni<sup>0</sup> peaks were detected for Ni65CS and Ni75CS. On the other hand, sharp and intense Ni<sup>0</sup> peaks can be seen on samples Ni85CS and NiCe catalysts, which is an evidence of larger average crystallite sizes.

After the reduction process, average Ni crystallite sizes were estimated for each catalyst using the Scherrer equation. The calculations were made considering  $2\theta = 51.8^\circ$ , since this Ni<sup>0</sup> peak has no interference from any ceria phase of the samples. Table 1 shows that Ni65CS and Ni75CS have similar average Ni crystallite sizes (around 30 nm), while Ni85CS (81.7 nm) and NiCe (113.1 nm) are considerably larger, which may influence their catalytic properties. Literature shows that catalysts with smaller particle sizes tend to have lower carbon formation rates and consequently higher stability (Lima et al., 2010).

Silica mass content might also have had an important role on the thermal stability of the catalysts and possibly on the interaction between NiO and the supports. Ni65CS (A) and Ni75CS (B) started their reduction process at higher temperatures (around 400 °C) than the other two samples (around 350 °C). These results suggest that NiO phase interacts stronger with the support when silica content was increased due to smaller average crystallites, which decreased their reducibility.

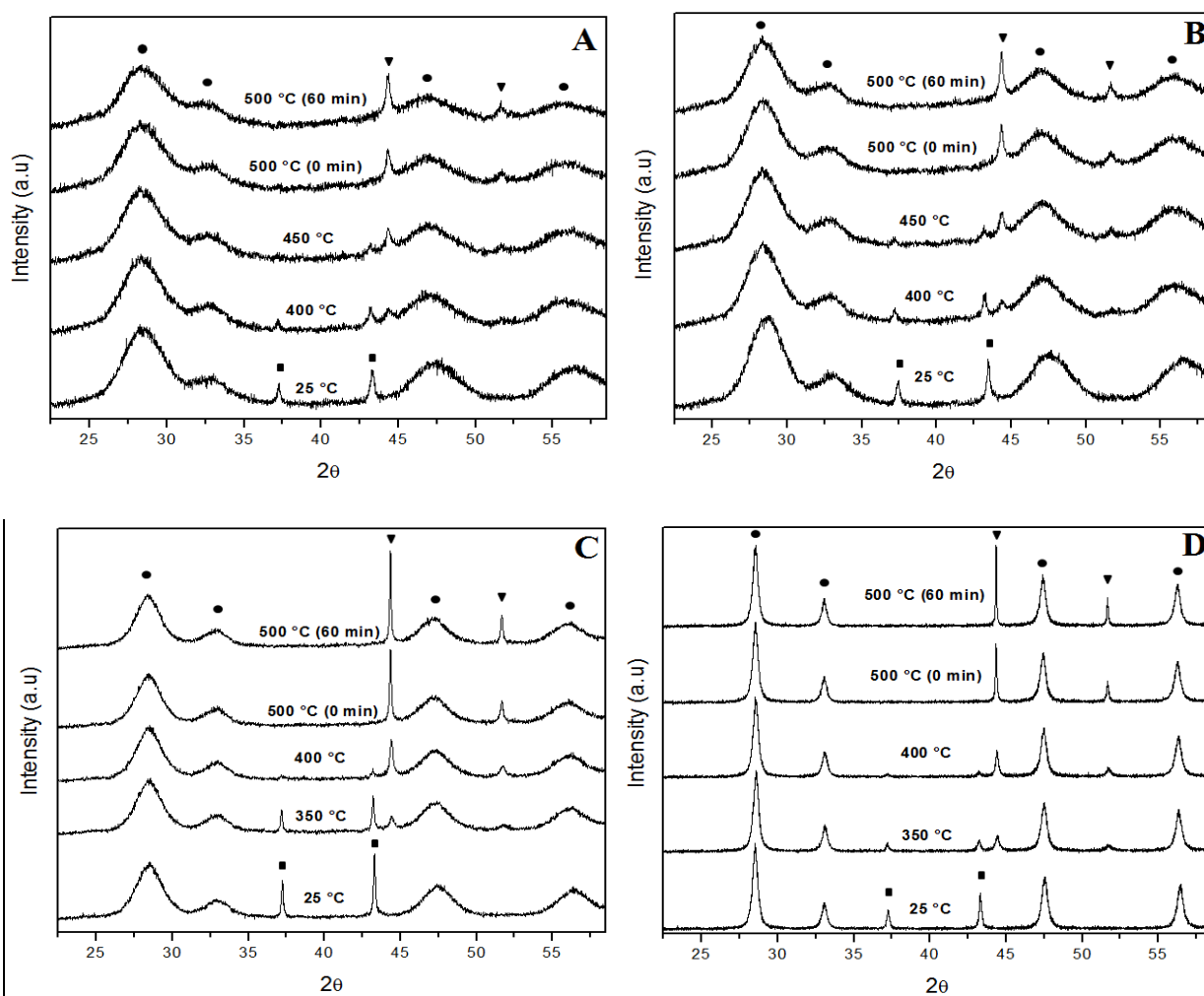


**Figure 4.1:** *in situ* XRD diffractograms of supported nickel precursors Ni65CS (A), Ni75CS (B), Ni85CS (C) and NiCe (D), where (■) NiO, (▼) Ni<sup>0</sup>, (●) CeO<sub>2</sub>.

BET results (Table 4.1) showed the effect of silica addition on the support concerning the surface area. The precursor supported over pure ceria (NiCe) showed a surface area 5 times smaller

than Ni85CS, which had a 15% molar addition of silica. Increasing silica molar content to 25 and 35% on Ni75CS and Ni65CS, respectively, provided these precursors a considerable higher area than Ni85CS. The enhancing area effect of silica addition favored a higher dispersion of Ni. The effects of silica addition over ceria-type supports can be easily found in literature (Yap et al., 2013, Trovarelli et al., 2001, Reddy et al., 2002).

CO<sub>2</sub>-TPD results are also summarized in Table 4.1. It can be noticed that silica addition to a ceria support increased the catalysts basicity, since NiCe presented the lowest quantity of desorbed CO<sub>2</sub> (77 μmol/g). However, the positive effect of silica addition on the catalyst basicity is limited. It was observed that there was a maximum value of desorbed CO<sub>2</sub> for Ni75CS (374 μmol/g), but when silica content was further increased to 35 wt.% (Ni65CS), the amount of desorbed CO<sub>2</sub> considerably decreased, indicating a drop on basicity.

**Table 4.1:** CO<sub>2</sub> TPD, BET area results and average Ni<sup>0</sup> particle size of ceria-silica supported Ni catalysts.

Samples	BET Area (m <sup>2</sup> /g)	D <sub>p</sub> Ni <sup>0</sup> (nm)	CO <sub>2</sub> TPD (μmol/g)
Ni65CS	160	30	297
Ni75CS	134	31	374
Ni85CS	75	82	132
NiCe	14	113	77

Figure 4.2 shows TPR profiles during the reduction of the calcined ceria-silica supported Ni precursors. It is possible to observe that all samples exhibit different kinds of hydrogen consumption peaks. The first one, between 200 and 300 °C for samples Ni85CS and NiCe, and between 200 and 350 °C, for samples Ni65CS and Ni75CS can be attributed to both the reduction of oxygen species in oxygen vacancies and the surface reduction of ceria (Das et al., 2018). The oxygen species adsorbed on these vacancies are easily reducible at low temperatures as can be seen in the TPR results. Furthermore, higher silica content on the support, and thus, the smaller ceria particles, may have increased this effect as the peaks are clearly bigger in precursors Ni65CS and Ni75CS, especially on the former one.

The second hydrogen consumption region of the samples is majorly related to the reduction of NiO. This consumption suffered a shift towards higher temperatures, around 400 °C, on samples Ni65CS and Ni75CS while on Ni85CS and NiCe it stood around 350 °C. This could be due to the effect of a higher content of silica in the former precursors, which might have granted a stronger interaction between NiO and the support as a consequence of smaller ceria particle sizes. These results are in accordance with the *in situ* XRD analysis since one could observe that the beginning of the Ni<sup>0</sup> phase formation on Ni65CS and Ni75CS started at higher temperatures than the other two samples. In their work, Zhao et al. (2016) also affirm that silica addition to the studied Ni/CeO<sub>2</sub> precursors led to an increase of NiO reduction temperature and the authors also attributed this behavior to a stronger metal-support interaction.

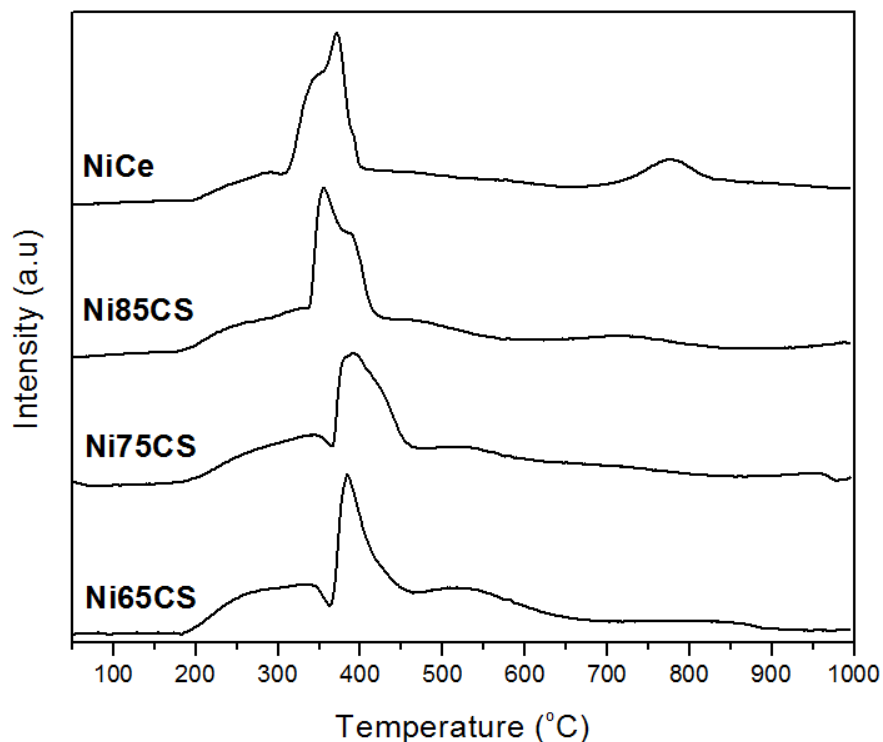


**Figure 4.2:** TPR profile of the ceria-silica supported Ni precursors.

The third hydrogen consumption peak in Ni65CS and Ni75CS reinforces silica content role in the reduction process, since they indicate that a great part of bulk ceria was reduced at lower temperatures, between 450 and 600 °C, while in NiCe precursor ceria reduction was observed only between 700 and 850 °C. Biswas et al. (2007) reported the same effect for their ceria-zirconia supports. According to their study the increasing of zirconia loadings on the support led to more



dispersed CeO<sub>2</sub> particles which had a direct effect on the reduction of bulk ceria at lower temperatures. Indeed, Trovarelli et al. (2001) showed the presence of silica directly affects ceria reducibility, but this behavior does not depend on structural perturbation in the lattice of ceria by the dopant. According to the authors, silica promotes the formation of small ceria crystallites, increasing ceria dispersion. Nanocrystalline ceria has a lower reduction energy compared to bulk ceria and thus can be reduced at lower temperatures.

Fig. 4.3 shows XANES results of ceria-silica supported Ni precursors Ni65CS (A), Ni75CS (B), Ni85CS (C) and NiCe (D) obtained in Ni K-edge. At room temperature, it is possible to observe a characteristic pre edge (around 8333 eV) in all samples, which can be attributed to a dipole 1s → 3d transition and it is commonly related to oxide-type phases (Gardner et al., 2010). Literature shows that the white line position can indicate the oxidation state of the analyzed elements.

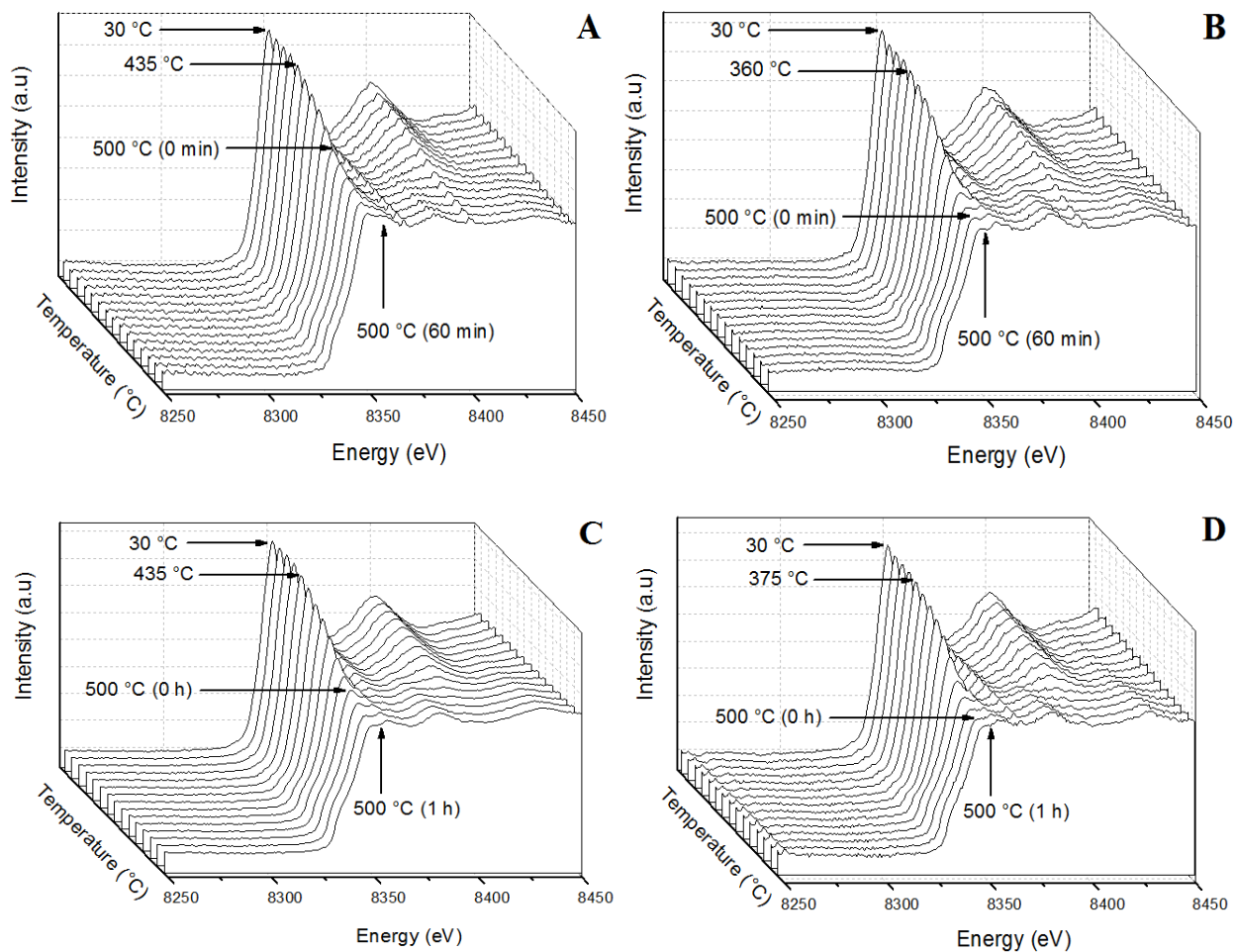


**Figure 4.3:** *in situ* XANES performed in Ni K-edge during the reduction process of supported nickel precursors Ni65CS (A), Ni75CS (B), Ni85CS (C) and NiCe (D).

Higher oxidation states are generally evidenced by a shift on the absorption peaks (Ávilla Neto et al., 2018). Because the white line absorption peak (around 8350 eV) is not shifted to higher energies, one might affirm that the highest and predominant Ni oxidation state is  $\text{Ni}^{2+}$ , as expected due to the presence of NiO in all samples. When temperature was gradually increased to 500 °C and in a reductive atmosphere it was observed a clear change on Ni patterns from  $\text{Ni}^{2+}$  to  $\text{Ni}^0$ . However, the white line intensity showed that sample Ni65CS was not totally reduced even after exposed to 500 °C for 60 min, since it slightly diverges from the used  $\text{Ni}^0$  reference (not shown). This result endorses *in situ* XRD and TPR analysis as it points out that the higher silica content in these precursors might have increased its thermal stability and therefore made it more difficult to reduce.

After the reduction procedure, all samples were evaluated during the steam reforming of propane (SRP) at 600 °C. The results showed that there were no changes in Ni oxidation state that remained on its metallic form even after 1 h of reaction for samples Ni75CS, Ni85CS and NiCe. Zimicz et al. (2017) found resembling results in their XANES study using ceria-zirconia supported Ni catalysts during the partial oxidation of methane. However, the same fact did not happen to Ni65CS (A) which suffered a variation in Ni oxidation state when temperature was increased to 600 °C, as can be seen in Figure 4.4. Based on the results, one may affirm that the higher temperature contributed to a complete reduction of Ni in this sample even in a reaction atmosphere.

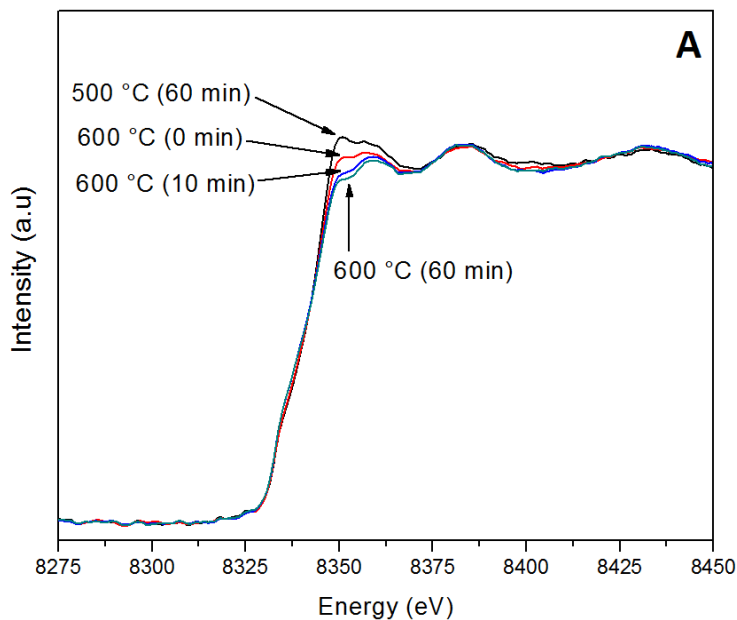


**Figure 4.4:** *in situ* XANES performed in Ni K-edge during the SRP reaction using the supported nickel catalyst Ni65CS (A).

Moreover, it is possible to infer that the complete reduction of Ni65CS has happened after 10 min at 600 °C and might have occurred due to the consumption of the produced hydrogen during the SRP. It is important to point out that in the reduction treatment at LNLS facility we used a 5%H<sub>2</sub>/He mixture due to safety issues and that could be the reason why this sample was not completely reduced at 500 °C. However, during the reduction process conducted before the catalytic tests a pure H<sub>2</sub> gas flow was used, which can ensure the full reduction of Ni species.

XANES analysis on Ce L<sub>III</sub>-edge was also conducted for ceria-silica supported Ni precursors Ni65CS (A), Ni75CS (B), Ni85CS (C) and NiCe (D) and the results can be seen in Fig. 4.5. At room temperature all samples showed characteristic Ce<sup>4+</sup> electronic configuration 4f<sup>0</sup> and 4f<sup>1</sup>, as can be seen by the peaks at 5730 and 5740 eV. When temperature was gradually increased to 500 °C, there was a clear drop in the absorption peak intensity (around 5740 eV) and a little shift of the peak around 5730 eV to 5728 eV for samples Ni65CS, Ni75CS and Ni85CS.

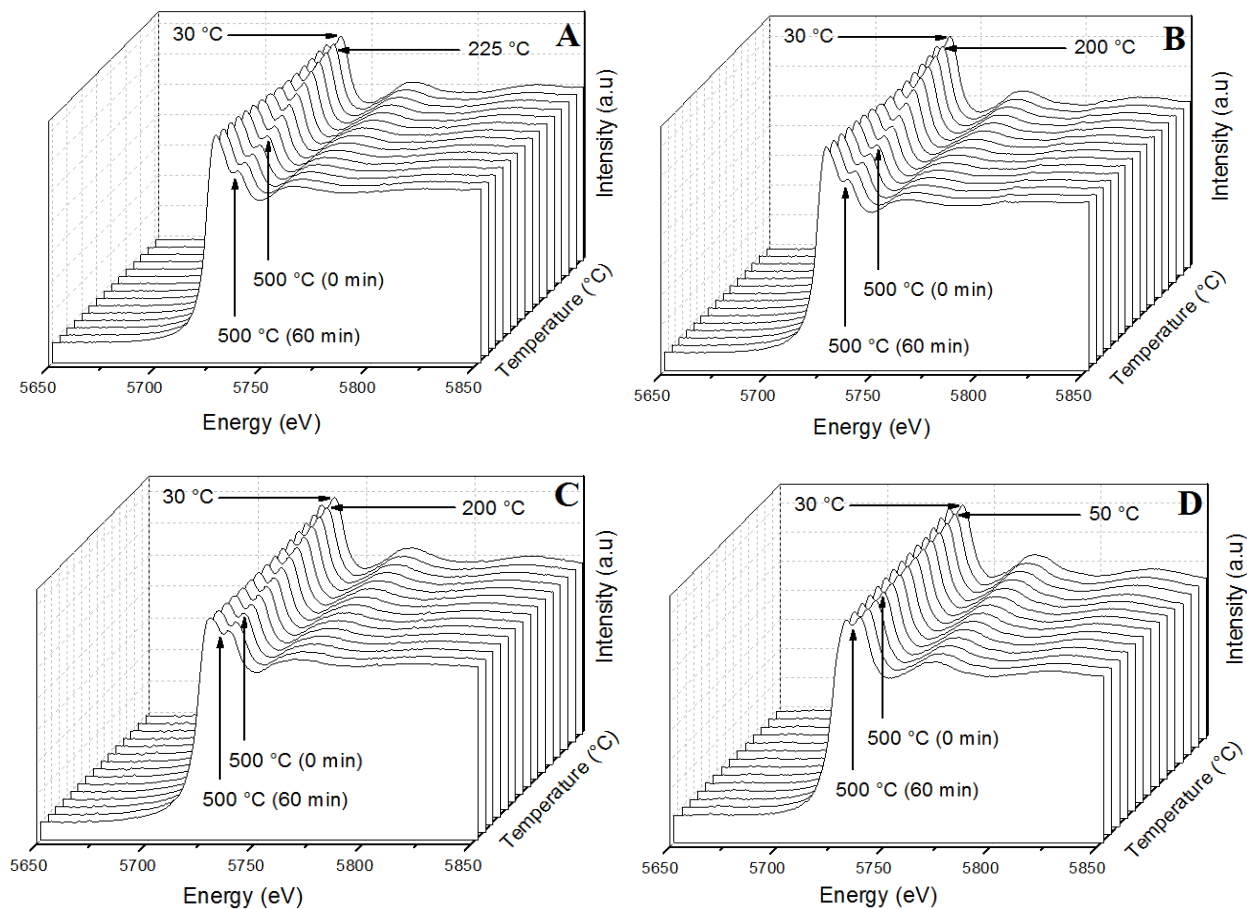


**Figure 4.5:** *in situ* XANES performed in Ce L<sub>III</sub>-edge during the reduction process of supported nickel precursors Ni65CS (A), Ni75CS (B), Ni85CS (C) and NiCe (D).

This behavior is related to the change of oxidation state from  $Ce^{4+}$  towards  $Ce^{3+}$ , and thus shows the reduction process of the support. The same behavior happened to NiCe but it was less evident than in the other precursors. Concerning the reduction temperature, sample Ni65CS started its support reduction process at the highest one (225 °C) while for Ni75CS and Ni85CS the reduction began at a slightly lower temperature (200 °C). On the other hand, NiCe showed a reduction start at only 50 °C. The obtained results are in accordance with the *in situ* XRD and TPR analysis, since they point out the influence of silica addition on the support, which contributes to the formation of smaller ceria particles and facilitates the reduction of ceria species. Resembling results were reported by Biswas et al. (2007), as discussed on TPR analysis. However, after exposed to 500 °C during 1 h in a reductive atmosphere all samples still exhibited a characteristic  $Ce^{4+}$  contribution, which was higher for NiCe and less intense for the other ceria-silica precursors. This indicates the presence of both  $Ce^{4+}$  and  $Ce^{3+}$  oxidation states in the supports even after the reduction process.

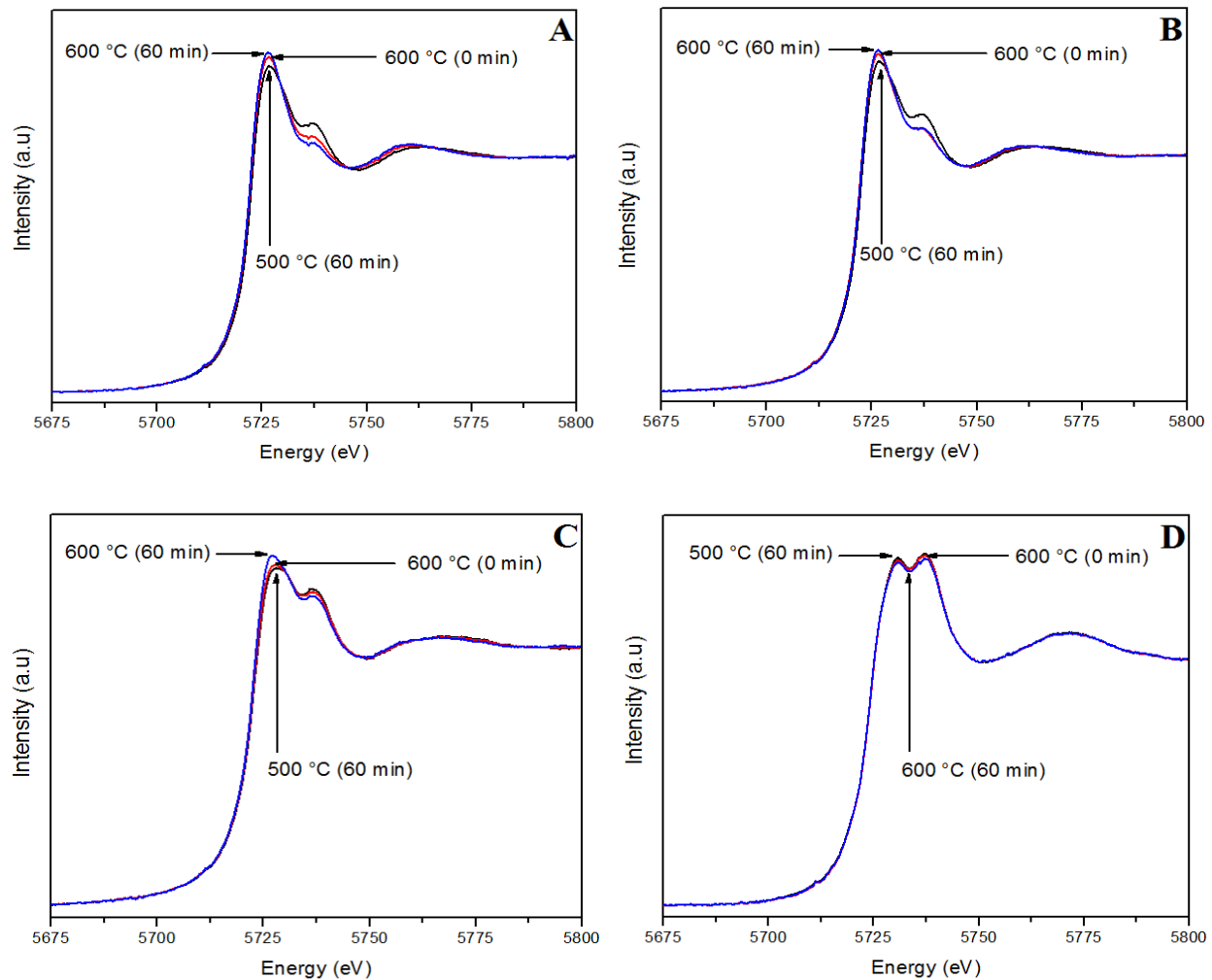


**Figure 4.6:** *in situ* XANES results in Ce L<sub>III</sub>-edge during the SRP reaction using ceria-silica supported nickel catalysts Ni65CS (A), Ni75CS (B), Ni85CS (C) and NiCe (D).

Samples Ni65CS (A), Ni75CS (B), Ni85CS (C) and NiCe (D) were also evaluated during the SRP at 600 °C on Ce L<sub>III</sub>-edge and the results were reported through Fig. 4.6. A similar effect of the temperature increase observed on Ni K-edge spectra also happened in the supports, i.e., even though the samples were exposed to a reaction atmosphere, the higher temperature and the produced hydrogen during the reaction made a higher reduction towards Ce<sup>3+</sup> possible. This effect was more explicit on Ni65CS and Ni75CS, which suffered both a considerable rise on Ce<sup>3+</sup> and a drop on Ce<sup>4+</sup> absorption peaks. The temperature effect was almost non-noticeable in NiCe, which corroborates to the TPR results since they showed that a considerable ceria bulk reduction was not expected below 700 °C.

#### 4.3.2. Stability Tests – Steam Reforming of Propane

Figs. 4.7 show the results of propane conversion at 600 °C and using a gas hourly space velocity (GHSV) of 1200 L/g<sub>Cat</sub>.h as a function of time-on-stream (TOS) for ceria-silica supported Ni catalysts. Silica addition in the support played an important role on the catalyst's stability, since there was a clear difference on the performances among the catalysts with higher silica content and the ones with lower (or none) silica content.

NiCe presented almost no activity and showed the lowest initial propane conversion (15%), which dropped to 5% before 10 h of TOS. Ni85CS also suffered from strong deactivation and after 25 h of TOS propane conversion dropped from 45 to 10%. There are basically three main reasons reported in literature for catalyst deactivation: particles sintering, coking and oxidation. It is unlikely sintering phenomenon has a big influence on these two samples since Ni particle size is considerably big right after the reduction process. Furthermore, BET, *in situ* XRD and TPR results indicated a direct influence of silica molar content on the dispersion of ceria and Ni particles. The poor dispersion of ceria particles allied to the large Ni crystallites in Ni85CS and NiCe (82 and 113 nm, respectively) caused a low metal-support interaction, which promotes the gradual oxidation of the catalysts active phase. Thus, we believe oxidation and carbon deposition are possibly the two main reasons to justify the low activity and poor stability observed in these samples.

Ni65CS and Ni75CS showed the highest initial conversion (70 and 65%, respectively) and remained stable after 25 h of TOS. The good performance of both catalysts is in agreement with *in situ* XRD, TPR and XANES characterization tests as the smaller average Ni crystallite size and the stronger metal-support interaction observed in these samples improved their stability and consequently avoided the catalysts deactivation. Moreover, the high activity presented by Ni65CS

and Ni75CS during the SRP also correlates to the CO<sub>2</sub>-TPD results, since their higher basicity contributes to a better catalytic performance. In their work, Yap et al. (2013) reported that the best conversion levels during the dry reforming of methane were achieved in the ceria-silica supported Ni catalysts with the highest basicity. According to the authors the enhanced number of basic sites of a catalyst favors the absorption and activation of hydrocarbons. The number of basic sites could be a possible explanation why Ni75CS showed a relative higher conversion rate of propane than Ni65CS, although both catalysts had similar Ni crystallite sizes.

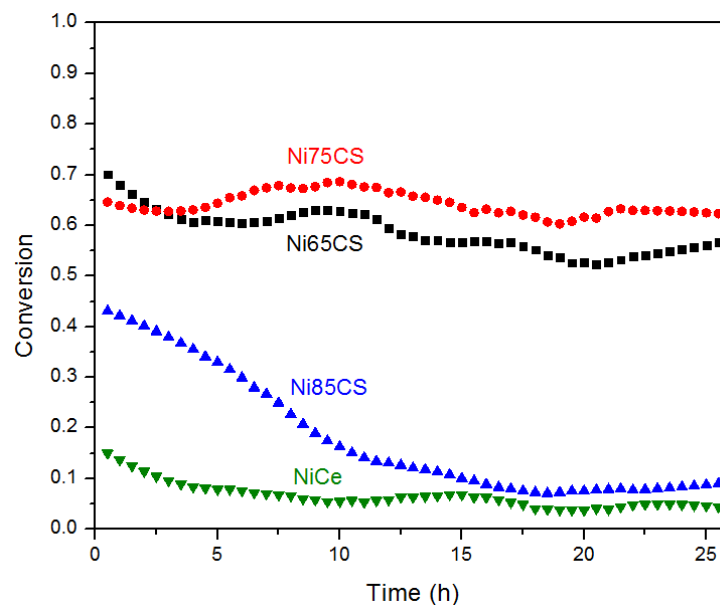


**Figure 4.7:** Propane conversion during the SRP at 600 °C over ceria-silica supported Ni catalysts, using a GHSV of 1200 L/g<sub>Cat</sub>.h.

Species molar fraction (dry basis) were also estimated during the steam reforming of propane (Figs. 4.8) for catalysts Ni65CS (A), Ni75CS (B), Ni85CS (C) and NiCe (D). The deactivation suffered by Ni85CS and NiCe was also observed on Figs. 4.8C and 4.8D. Hydrogen molar fraction measured for Ni85CS slowly decreases in the first 7 h of reaction, but after that rapidly drops and becomes smaller than propane's. CO<sub>2</sub> molar fraction also presented the same behavior and dropped from 15 to 5%. For NiCe, H<sub>2</sub> molar fraction strongly drops from 45 to 15% in the first 5h of reaction. After 17 h it was noticeable that propane molar fraction was around 95% while CO and CO<sub>2</sub> were practically undetectable, which indicates that the catalyst had no activity.

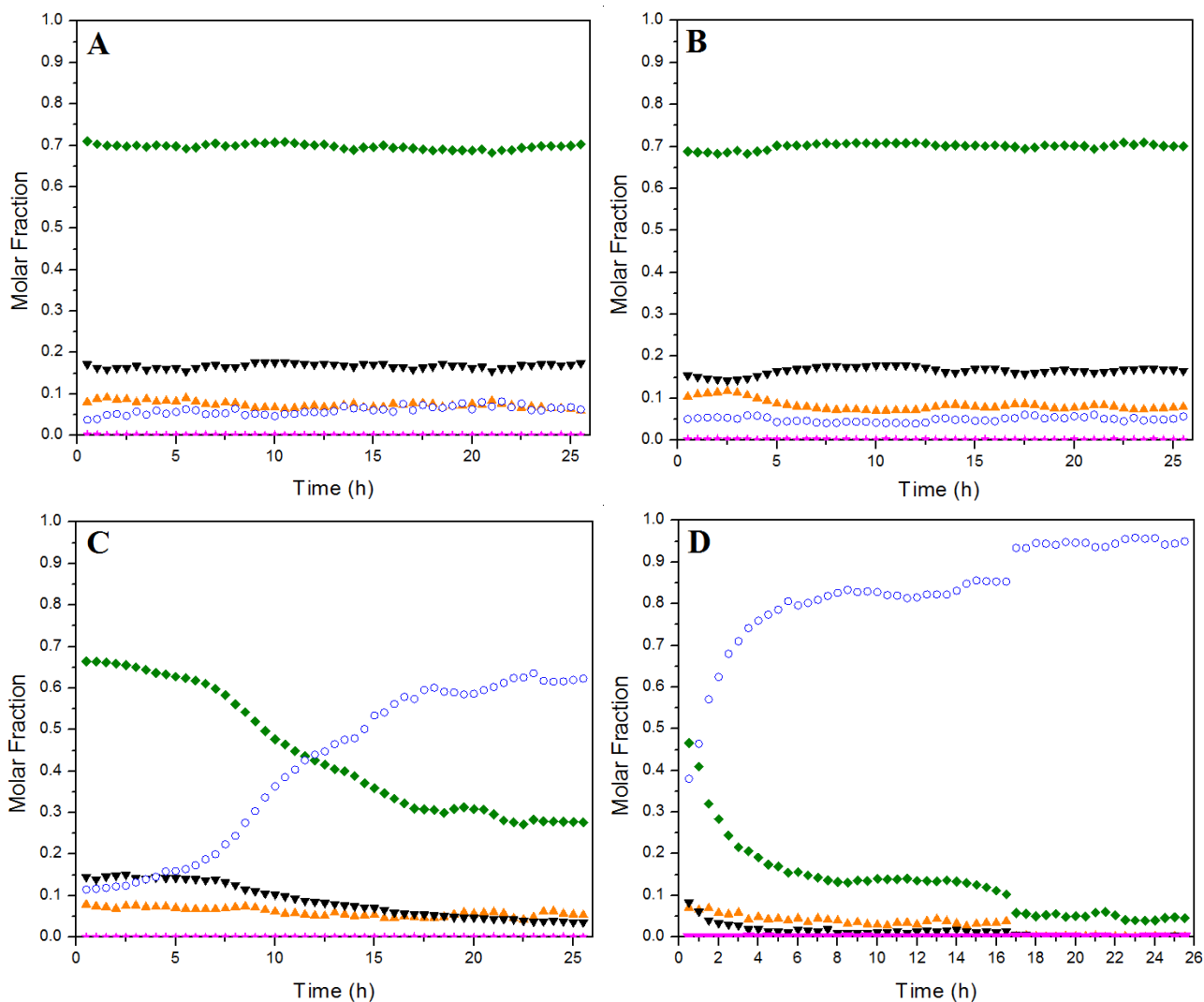


**Figure 4.8:** Species molar fraction during the SRP at 600 °C over ceria-silica supported Ni catalysts Ni65CS (A), Ni75CS (B), Ni85CS (C) and NiCe (D) using a GHSV of 1200 L/g<sub>cat</sub>.h, where (○) Propane, (◆) H<sub>2</sub>, (▼) CO<sub>2</sub>, (▲) CO and (★) CH<sub>4</sub>.

Ni65CS and Ni75CS presented relatively similar average molar fractions of H<sub>2</sub>, CO and CO<sub>2</sub> which remained stable during the analyzed TOS. Since both catalysts present close conversion rates (average gap of only 5%) and relatively similar molar fractions of species during the SRP, it could be stated that they have the same activity. In order to completely differ Ni65CS and Ni75CS the SRP was conducted at a lower temperature (400 °C) to ensure a kinetic regime operation. The conversion data obtained during this analysis was used to estimate propane reaction rate ( $R_p$ ) of each catalyst, including Ni85CS and NiCe (for comparison purposes) and the results are reported on Table 4.2.

**Table 4.2:** Estimated propane reaction rate of ceria-silica supported Ni catalysts at 400 °C.

Samples	$R_P$ (mols.g <sub>cat</sub> <sup>-1</sup> .h <sup>-1</sup> ) x 10 <sup>-3</sup>
Ni65CS	1.3
Ni75CS	2.3
Ni85CS	0.8
NiCe	0.6

The results show that propane consumption in the SR reaction for Ni75CS is almost 2 times higher than Ni65CS, which indicates the former catalyst is more active than the later one. As expected, Ni85CS and NiCe presented relatively low reaction rates, which is in accordance with the previous stability tests results conducted at 600 °C.

#### 4.3.3. Thermogravimetric Analysis (TGA)

TGA analysis of the used samples was conducted after the stability tests in order to evaluate the amount of deposited carbon over the catalysts. The results are reported in Table 4.3.

**Table 4.3:** Estimated carbon formation rate of the spent ceria-silica supported Ni catalysts.

Samples	Carbon formation rate (mg C/g <sub>cat</sub> .h.g <sub>C.react</sub> )
Ni65CS	3.3
Ni75CS	6.3
Ni85CS	7.8
NiCe	2.7

The results showed that NiCe had the lowest carbon formation rate, which is justified by the poor activity of the catalyst. Besides, because of the low carbon deposition on this sample one might infer that oxidation of the metallic phase was the main cause of its deactivation. Oppositely, Ni85CS showed the highest carbon formation rate which might explain its gradual deactivation. That corroborates to the species molar fraction results (Fig. 4.8 C) where it is possible to notice a gradual drop in CO<sub>2</sub> molar fraction, which could indicate a loss of the catalyst capacity to gasify the deposited carbon.



The carbon formation rate for Ni75CS was considerably higher than for Ni65CS. The higher activity of the former sample due to the larger number of basic sites might have contributed to the higher carbon formation on the catalyst surface. At the same time, the higher silica molar content in Ni65CS may have caused a greater dispersion of ceria particles, which facilitates ceria reducibility, increases oxygen mobility in the support and favors the lower carbon deposition on the catalyst surface. This hypothesis is in accordance with XANES results on Ce L<sub>III</sub>-edge during the SRP (Figs. 4.6 A and B), where it was possible to notice that ceria was slightly more reduced (absorption peak behavior towards Ce<sup>3+</sup>) on Ni65CS than on Ni75CS. Furthermore, Trovarelli et al. (2001) have reported the positive effect of silica addition on ceria materials dispersion. More recently, Zhao et al. (2016) confirmed silica influence on ceria particles dispersion in their work on dry reforming of methane using ceria-based supported Ni catalysts. The authors observed an improvement on their Ni/CeO<sub>2</sub> catalysts concerning activity, stability and coke resistance when silica was added to the system and they attributed the noted better performance to the formation of well dispersed ceria particles. According to them, the formation of nanocrystalline ceria allows more oxygen vacancies on the support, which act towards carbon gasification and clean the catalytic surface.

#### 4.4. Conclusions

This work evaluated the influence of different silica molar contents on ceria materials used as supports of Ni catalytic precursors. Four precursors were characterized and afterwards tested during the steam reforming of propane, used as a model molecule for LPG. Characterization tests pointed out that ceria-silica supported Ni catalysts (Ni/xCS) showed better properties than Ni/CeO<sub>2</sub> (NiCe) in terms of catalytic area, average Ni crystallite size, reducibility and basicity. It was observed through BET area, *in situ* XRD, TPR and XANES results that a higher silica molar content in the support brought a higher strength on the metal-support interaction as a consequence of smaller particle sizes, which reflected on the reduction temperature of the samples. TPR, XANES and TGA indicated that carbon deposition rate of the samples and the reducibility of ceria materials had a direct influence of silica molar content on the precursors. A higher silica content (especially on Ni65CS and Ni75CS) contributed to increasing ceria dispersion on the support and facilitated oxygen mobility, which contributed to carbon species gasification and cleaning the catalyst surface. Stability tests showed that Ni65CS and Ni75CS remain stable and active during the analyzed TOS and had close performances. However, the later presented considerably more basic sites on CO<sub>2</sub>-TPD results, which contributed to a higher conversion rate of propane at 600 °C.

## References

- H.F. Abbas, W.M.A. Wan Daud, Hydrogen production by methane decomposition: A review. *Int. J. Hydrogen Energy*, 35 (2010) 1160-90.  
<https://doi.org/10.1016/j.ijhydene.2009.11.036>
- A.L. Alberton, M.M.V.M. Souza, M. Schmal. Carbon formation and its influence on ethanol steam reforming over Ni/Al<sub>2</sub>O<sub>3</sub> catalysts. *Catal Today* 123 (2007) 257-64.  
<https://doi.org/10.1016/j.cattod.2007.01.062>
- M.C. Alvarez-Galvan, D.A. Constantinou, R. M. Navarro, J. A. Villoria, J. L. G. Fierro, A. M. Efstathiou. Surface reactivity of LaCoO<sub>3</sub> and Ru/LaCoO<sub>3</sub> towards CO, CO<sub>2</sub> and C<sub>3</sub>H<sub>8</sub>: effect of H<sub>2</sub> and O<sub>2</sub> pretreatments. *Appl. Catal. B*, 102 (2011) 291-301.  
<https://doi.org/10.1016/j.apcatb.2010.12.015>
- M.H. Amin, S. Putla, S.B.A. Hamid, S.K. Bhargava, Understanding the role of lanthanide promoters on the structure–activity of nanosized Ni/-Al<sub>2</sub>O<sub>3</sub> catalysts in carbon dioxide reforming of methane. *Appl. Catal. A*, 492 (2015) 160–68.  
<https://doi.org/10.1016/j.apcata.2014.12.038>
- A. K. Avci, Z. I. Önsan, D. L. Trimm, On-board fuel conversion for hydrogen fuel cells: comparison of different fuels by computer simulations. *Appl. Catal. A*, 216 (2001) 243–56.  
[https://doi.org/10.1016/S0926-860X\(01\)00568-3](https://doi.org/10.1016/S0926-860X(01)00568-3)
- A. K. Avci, D. L. Trimm, A. E. Aksoylu, Z. I. Önsan, Hydrogen production by steam reforming of *n*-butane over supported Ni and Pt-Ni catalysts. *Appl. Catal. A*, 258 (2004) 235–40.  
<https://doi.org/10.1016/j.apcata.2003.09.016>
- C.N. Ávila-Neto, K.D. Oliveira, K.F. Oliveira, A.M.M. Arouca, R.A.R. Ferreira, C.E. Hori, Interconnection between feed composition and Ni/Co ratio in (La-Ni-Co-O)-based perovskites and its effects on the stability of LPG steam reforming. *Appl. Catal. A*, 550 (2018) 184 – 97.  
<https://doi.org/10.1016/j.apcata.2017.11.011>
- J. Bae, S. Lee, S. Kim, J. Oh, S. Choi, M. Bae, I. Kang, S.P. Katikaneni, Liquid fuel processing for hydrogen production: A review. *Int. J. Hydrogen Energy* 41 (2016) 19990 – 20022.  
<https://doi.org/10.1016/j.ijhydene.2016.08.135>
- A.C. Basagiannis, X.E. Verykios. Reforming reactions of acetic acid on nickel catalysts over a wide temperature range. *Appl. Catal. A*, 308 (2006) 182-93.  
<https://doi.org/10.1016/j.apcata.2006.04.024>

P. Biswas, D. Kunzru, Steam reforming of ethanol for production of hydrogen over Ni/CeO<sub>2</sub>-ZrO<sub>2</sub> catalyst: Effect of support and metal loading. *Int. J. Hydrogen Energy* 32 (2007) 969 – 80.

<https://doi.org/10.1016/j.ijhydene.2006.09.031>

R.P. Borges, R.A.R. Ferreira, R.C. Rabelo-Neto, F.B. Noronha, C.E. Hori, Hydrogen production by steam reforming of acetic acid using hydrotalcite type precursors. *Int. J. Hydrogen Energy* 43 (2018) 7881 – 92.

<https://doi.org/10.1016/j.ijhydene.2018.03.028>

T. Borowiecki, W. Grzegorzczak, A. Denis, A. Golebiowski, Resistance to coking determination by temperature programmed reaction of n-butane with steam. *Catal. Lett.* 79 (2002) 1 – 4.

<https://doi.org/10.1023/A:1015332031458>

P.K. Cheekatamarla, C.M. Finnerty, Reforming catalysts for hydrogen generation in fuel cell applications. *J. Power Sources* 160 (2006) 490 – 99.

<https://doi.org/10.1016/j.jpowsour.2006.04.078>

Y. Chen, J. Ren, Conversion of methane and carbon dioxide into synthesis gas over alumina-supported nickel catalysts. Effect of Ni-Al<sub>2</sub>O<sub>3</sub> interactions. *Catal. Lett.* 29 (1994) 39 – 48.

<https://doi.org/10.1007/BF00814250>

S. O. Choi, S. H. Moon, Performance of La<sub>1-x</sub>Ce<sub>x</sub>Fe<sub>0.7</sub>Ni<sub>0.3</sub>O<sub>3</sub> perovskite catalysts for methane steam reforming. *Catal. Today* 146 (2009) 148 – 53.

<https://doi.org/10.1016/j.cattod.2009.02.023>

S. Das, J. Ashok, Z. Bian, N. Dewangan, M.H. Wai, Y. Du, A. Borgna, K. Hidajat, S. Kawi, Silica-Ceria sandwiched Ni core-shell catalyst for low temperature dry reforming of biogas: Coke resistance and mechanistic insights. *Appl. Catal. B*, 230 (2018) 220–236.

<https://doi.org/10.1016/j.apcatb.2018.02.041>

E.C. Faria, R.C. Rabelo-Neto, R.C. Colman, R.A.R. Ferreira, C.E. Hori, F.B. Noronha, Steam Reforming of LPG over Ni/Al<sub>2</sub>O<sub>3</sub> and Ni/Ce<sub>x</sub>Zr<sub>1-x</sub>O<sub>2</sub>/Al<sub>2</sub>O<sub>3</sub> Catalysts. *Catal. Lett.* 146 (2016) 2229–41.

<https://doi.org/10.1007/s10562-016-1833-3>

W.L.S. Faria, L.C. Dieguez, M. Schmal, Autothermal reforming of propane for hydrogen production over Pd/CeO<sub>2</sub>/Al<sub>2</sub>O<sub>3</sub> catalysts. *Appl. Catal. B*, 85 (2008) 77–85.

<https://doi.org/10.1016/j.apcatb.2008.06.031>

L.S.F. Feio, C.E. Hori, S. Damyanova, F.B. Noronha, W.H. Cassinelli, C.M.P. Marques, J.M.C. Bueno, The effect of ceria content on the properties of Pd/CeO<sub>2</sub>/Al<sub>2</sub>O<sub>3</sub> catalysts for steam reforming of methane. *Appl. Catal. A*, 316 (2007) 107–16.

<https://doi.org/10.1016/j.apcata.2006.09.032>

R.A.R. Ferreira, C.N. Avila-Neto, F.B. Noronha, C.E. Hori. Study of LPG steam reform using Ni/Mg/Al hydrotalcite-type precursors. *Int J Hydrogen Energy*, 44 (2019) 24471-84.

<https://doi.org/10.1016/j.ijhydene.2019.07.193>

J.L.G. Fierro, J.M.D. Tascón, L.G. Thijca, Surface Properties of LaNiO<sub>3</sub>: Kinetic Studies of Reduction and of Oxygen Adsorption. *J. Catal.* 93 (1985) 83 – 91.

[https://doi.org/10.1016/0021-9517\(85\)90153-8](https://doi.org/10.1016/0021-9517(85)90153-8)

T.H. Gardner, J.J. Spivey, A. Campos, J.C. Hissam, E.L. Kugler, A.D. Roy, Catalytic partial oxidation of CH<sub>4</sub> over Ni-substituted barium hexaaluminate catalysts. *Catal. Today* 157 (2010) 166–69. <https://doi.org/10.1016/j.cattod.2010.05.033>

F. Gökaliler, Z.I. Önsan, A.E. Aksoylu, Power-law type rate equation for propane ATR over Pt–Ni/Al<sub>2</sub>O<sub>3</sub> catalyst. *Int. J. Hydrogen Energy* 37 (2012) 10425 – 9.

<https://doi.org/10.1016/j.ijhydene.2012.01.114>

D. Harshini, C.W. Yoon, J. Han, S.P. Yoon, S.W. Nam, T. Lim, Catalytic Steam Reforming of Propane over Ni/LaAlO<sub>3</sub> Catalysts: Influence of Preparation Methods and OSC on Activity and Stability. *Catal. Lett.* 142 (2012) 205–12.

<https://doi.org/10.1007/s10562-011-0746-4>

A. Haryanto, S. Fernando, N. Murali, S. Adhikari, Current Status of Hydrogen Production Techniques by Steam Reforming of Ethanol: A Review. *Energ. Fuel.* 19 (2005) 2098 – 106.

<https://doi.org/10.1021/ef0500538>

J. He, X.H. Lu, Y. Shen, R. Jing, R.-F. Nie, D. Zhou, Q.-H. Xia, Highly selective hydrogenation of phenol to cyclohexanol over nano silica supported Ni catalysts in aqueous medium. *Mol. Catal.* 440 (2017) 87 – 95.

<https://doi.org/10.1016/j.mcat.2017.07.016>

J. Hu, C. Yu, Y. Bi, L. Wei, J. Chen, X. Chen, Preparation and characterization of Ni/CeO<sub>2</sub>-SiO<sub>2</sub> catalysts and their performance in catalytic partial oxidation of methane to syngas. *Chinese J. Catal.* 35 (2014) 8–20.

[https://doi.org/10.1016/S1872-2067\(12\)60723-2](https://doi.org/10.1016/S1872-2067(12)60723-2)

X. Hu, G. Lu, Comparative study of alumina-supported transition metal catalysts for hydrogen generation by steam reforming of acetic acid. *Appl. Catal. B*, 99 (2010) 289–97.

<https://doi.org/10.1016/j.apcatb.2010.06.035>

T. Huang, H. Lin, T. Yu, A comparison of oxygen-vacancy effect on activity behaviors of carbon dioxide and steam reforming of methane over supported nickel catalysts. *Catal. Lett.* 105 (2005) 239

– 47. <https://doi.org/10.1007/s10562-005-8697-2>

U. Izquierdo, V.L. Barrio, J.F. Cambra, J. Requies, M.B. Guemez, P.L. Arias, G. Kolb, R. Zapf, A.M. Gutierrez, J.R. Arraibi, Hydrogen production from methane and natural gas steam reforming in conventional and micro reactor reaction systems. *Int J. Hydrogen Energy* 37 (2012) 7026-33.

<https://doi.org/10.1016/j.ijhydene.2011.11.048>

G. Jacobs, R.A. Keogh, B.H. Davis, Steam reforming of ethanol over Pt/ceria with co-fed hydrogen. *J. Catal.* 245 (2007) 326 – 37.

<https://doi.org/10.1016/j.jcat.2006.10.018>

H. Jeong, M. Kang, Hydrogen production from butane steam reforming over Ni/Ag loaded MgAl<sub>2</sub>O<sub>4</sub> catalyst. *Appl. Catal. B*, 95 (2010) 446 – 55.

<https://doi.org/10.1016/j.apcatb.2010.01.026>

Q. Jing, H. Lou, J. Fei, Z. Hou, X. Zheng, Syngas production from reforming of methane with CO<sub>2</sub> and O<sub>2</sub> over Ni/SrO–SiO<sub>2</sub> catalysts in a fluidized bed reactor. *Int. J. Hydrogen Energy* 29 (2004) 1245 – 51.

<https://doi.org/10.1016/j.ijhydene.2004.01.012>

T. Johansson, D. Pakhare, D. Haynes, V. Abdelsayed, D. Shekhawat, J. Spivey, Characterization of LaRhO<sub>3</sub> perovskites for dry (CO<sub>2</sub>) reforming of methane (DRM). *Chem. Pap.* 68, 9 (2014) 1240 –

47. <https://doi.org/10.2478/s11696-014-0566-2>

N. Kumar, A. Roy, Z. Wang, E.M. L'Abbate, D. Haynes, D. Shekhawat, J.J. Spivey, Bi-reforming of methane on Ni-based pyrochlore catalyst. *Appl. Catal. A*, 215 (2016) 211-16.

<https://doi.org/10.1016/j.apcata.2016.03.016>

N. Laosiripojana, W. Sutthisripok, S. Charojrochkul, S. Assabumrungrat, Steam reforming of LPG over Ni and Rh supported on Gd–CeO<sub>2</sub> and Al<sub>2</sub>O<sub>3</sub>: Effect of support and feed composition. *Fuel* 90 (2011) 136 – 41.

<https://doi.org/10.1016/j.fuel.2010.07.053>

N. Laosiripojana, W. Sutthisripok, P. Kim-Lohsoontorn, S. Assabumrungrat, Reactivity of Ce-ZrO<sub>2</sub> (doped with La-, Gd-, Nb-, and Sm-) toward partial oxidation of liquefied petroleum gas: Its application for sequential partial oxidation/steam reforming. *Int. J. Hydrogen Energy* 35 (2010) 6747–56.

<https://doi.org/10.1016/j.ijhydene.2010.04.095>

N. Laosiripojana, S. Assabumrungrat, Hydrogen production from steam and autothermal reforming of LPG over high surface area ceria. *J. Power Sources* 158 (2006) 1348–1357.

<https://doi.org/10.1016/j.jpowsour.2005.10.058>

N. Laosiripojana, S. Assabumrungrat, Methane steam reforming over Ni/Ce–ZrO<sub>2</sub> catalyst: Influences of Ce–ZrO<sub>2</sub> support on reactivity, resistance toward carbon formation, and intrinsic reaction kinetics. *Appl. Catal. A*, 290 (2005) 200 – 11.

<https://doi.org/10.1016/j.apcata.2005.05.026>

T.L. LeValley, A.R. Richard, M. Fan, The progress in water gas shift and steam reforming hydrogen production technologies: A review. *Int. J. Hydrogen Energy* 39 (2014) 16983 – 17000.

<https://doi.org/10.1016/j.ijhydene.2014.08.041>

Y. Li, L. Guo, X. Zhang, H. Jin, Y. Lu, Hydrogen production from coal gasification in supercritical water with a continuous flowing system. *Int. J. Hydrogen Energy* 35 (2010) 3036-45.

<https://doi.org/10.1016/j.ijhydene.2009.07.023>

Z. Li, X. Hu, L. Zhang, S. Liu, G. Lu, Steam reforming of acetic acid over Ni/ZrO<sub>2</sub> catalysts: Effects of nickel loading and particle size on product distribution and coke formation, *Appl. Catal. A*, 417–418 (2012) 281-89.

<https://doi.org/10.1016/j.apcata.2012.01.002>

S.M. de Lima, M.A. Peña, J.L.G. Fierro, J.M. Assaf, La<sub>1-x</sub>Ca<sub>x</sub>NiO<sub>3</sub> Perovskite Oxides: Characterization and Catalytic Reactivity in Dry Reforming of Methane. *Catal. Lett.* 124 (2008) 195 – 203. <https://doi.org/10.1007/s10562-008-9484-7>

S.M. Lima, A.M. Silva, L.O.O. Costa, J.M. Assaf, G. Jacobs, B.H. Davis, L.V. Mattos, F.B. Noronha, Evaluation of the performance of Ni/La<sub>2</sub>O<sub>3</sub> catalyst prepared from LaNiO<sub>3</sub> perovskite-type oxides for the production of hydrogen through steam reforming and oxidative steam reforming of ethanol. *Appl. Catal. A*, 377 (2010) 181–90.

<https://doi.org/10.1016/j.apcata.2010.01.036>

C. Liu, J. Ye, J. Jiang, Y. Pan, Progresses in the Preparation of Coke Resistant Ni-based Catalyst for Steam and CO<sub>2</sub> Reforming of Methane. *ChemCatChem*, 3 (2011) 529 – 41.

<https://doi.org/10.1002/cctc.201000358>

Z.O. Malaibari, A. Amin, E. Croiset, W. Epling. Performance characteristics of Mo-Ni/Al<sub>2</sub>O<sub>3</sub> catalysts in LPG oxidative steam reforming for hydrogen production. *Int. J. Hydrogen Energy*, 39 (2014) 10061 – 73.

<https://doi.org/10.1016/j.ijhydene.2014.03.169>

S.S. Maluf, E.M. Assaf, Ni catalysts with Mo promoter for methane steam reforming. *Fuel*, 88 (2009) 1547–53.

<https://doi.org/10.1016/j.fuel.2009.03.025>

V.B. Mortola, S. Damyanova, D. Zanchet, J.M.C. Bueno, Surface and structural features of Pt/CeO<sub>2</sub>-La<sub>2</sub>O<sub>3</sub>-Al<sub>2</sub>O<sub>3</sub> catalysts for partial oxidation and steam reforming of methane. *Appl. Catal. B*, 107 (2011) 221– 36.

<https://doi.org/10.1016/j.apcatb.2011.07.012>

N.Z. Muradov, T. N. Veziroglu, “Green” path from fossil-based to hydrogen economy: An overview of carbon-neutral technologies. *Int. J. Hydrogen Energy* 33 (2008) 6804-39.

<https://doi.org/10.1016/j.ijhydene.2008.08.054>

S. Natesakhawat, R.B. Watson, X. Wang, U.S. Ozkan, Deactivation characteristics of lanthanide-promoted sol-gel Ni/Al<sub>2</sub>O<sub>3</sub> catalysts in propane steam reforming. *J. Catal.* 234 (2005) 496–508.

<https://doi.org/10.1016/j.jcat.2005.07.014>

B. Nematollahi, M. Rezaei, E.N. Lay, Selective methanation of carbon monoxide in hydrogen rich stream over Ni/CeO<sub>2</sub> nanocatalysts. *J. Rare Earths* 33 2015 619 – 28.

[https://doi.org/10.1016/S1002-0721\(14\)60462-2](https://doi.org/10.1016/S1002-0721(14)60462-2)

M. Ni, M.K.H. Leung, D.Y.C. Leung, K. Sumathy, A review and recent developments in photocatalytic water-splitting using TiO<sub>2</sub> for hydrogen production. *Renew. Sust. Energ. Rev.*, 11 (2007) 401–25.

<https://doi.org/10.1016/j.rser.2005.01.009>

F.G.E. Nogueira, P.G.M. Assaf, H.W.P. Carvalho, E.M. Assaf, Catalytic steam reforming of acetic acid as a model compound of bio-oil, *Appl. Catal. B*, 160 (2014) 188–99.

<https://doi.org/10.1016/j.apcatb.2014.05.024>

- U. Oemar, P.S. Ang, K. Hidajat, S. Kawi, Promotional effect of Fe on perovskite  $\text{LaNi}_x\text{Fe}_{1-x}\text{O}_3$  catalyst for hydrogen production via steam reforming of toluene. *Int J. Hydrogen Energy* 38 (2013) 5525 – 34. <https://doi.org/10.1016/j.ijhydene.2013.02.083>
- S.T. Oyama, P. Hacırlıoğlu, Y. Gu, D. Lee, Dry reforming of methane has no future for hydrogen production: Comparison with steam reforming at high pressure in standard and membrane reactors. *Int. J. Hydrogen Energy*, 37 (2012) 10444 – 50.  
<https://doi.org/10.1016/j.ijhydene.2011.09.149>
- R. Pereñíguez, V.M. Gonzalez-delaCruz, A. Caballero, J.P. Holgado.  $\text{LaNiO}_3$  as a precursor of  $\text{Ni/La}_2\text{O}_3$  for  $\text{CO}_2$  reforming of  $\text{CH}_4$ : Effect of the presence of amorphous  $\text{NiO}$  phase. *Appl. Catal. B*, 123-124 (2012) 324 – 32.  
<https://doi.org/10.1016/j.apcatb.2012.04.044>
- R. Pereñíguez, V.M. González-DelaCruz, J.P. Holgado, A. Caballero, Synthesis and characterization of a  $\text{LaNiO}_3$  perovskite as precursor for methane reforming reactions catalysts. *Appl. Catal. B*, 93, 3-4 (2010) 346 – 53.  
<https://doi.org/10.1016/j.apcatb.2009.09.040>
- R.C. Rabelo-Neto, H.B.E. Sales, C.V.M. Inocência, E. Varga, A. Oszko, A. Erdohelyi, F.B. Noronha, L.V. Mattos,  $\text{CO}_2$  reforming of methane over supported  $\text{LaNiO}_3$  perovskite-type oxides. *Appl. Catal. B*, 221 (2018) 349–61.  
<https://doi.org/10.1016/j.apcatb.2017.09.022>
- L. Raslavičius, A. Keršys, S. Mockus, N. Keršienė, M. Starevičius, Liquefied petroleum gas (LPG) as a medium-term option in the transition to sustainable fuels and transport. *Renew. Sust. Energ. Rev.*, 32 (2014) 513–25.  
<https://doi.org/10.1016/j.rser.2014.01.052>
- B.M. Reddy, A. Khan, Nanosized  $\text{CeO}_2\text{-SiO}_2$ ,  $\text{CeO}_2\text{-TiO}_2$ , and  $\text{CeO}_2\text{-ZrO}_2$  mixed oxides: influence of supporting oxide on thermal stability and oxygen storage properties of ceria. *Catal. Surv. Asia* 9 (2005) 155 – 71.  
<https://doi.org/10.1007/s10563-005-7552-1>
- B.M. Reddy, A. Khan, Y. Yamada, T. Kobayashi, S. Loridant, J. C. Volta, Structural Characterization of  $\text{CeO}_2\text{-TiO}_2$  and  $\text{V}_2\text{O}_5/\text{CeO}_2\text{-TiO}_2$  Catalysts by Raman and XPS Techniques. *J. Phys. Chem. B*, 107 (2003) 5162 – 67.  
<https://doi.org/10.1021/jp0344601>



K.A. Resende, C.N. Ávila-Neto, R.C. Rabelo-Neto, F.B. Noronha, C.E. Hori, Hydrogen production by reforming of acetic acid using La–Ni type perovskites partially substituted with Sm and Pr. *Catal. Today*, 242 (2015) 71–9.

<https://doi.org/10.1016/j.cattod.2014.07.013>

M.C. Ribeiro, G. Jacobs, B.H. Davis, L.V. Mattos, F.B. Noronha, Ethanol Steam Reforming: Higher Dehydrogenation Selectivities Observed by Tuning Oxygen-Mobility and Acid/Base Properties with Mn in CeO<sub>2</sub>.MnO<sub>x</sub>.SiO<sub>2</sub> Catalysts. *Top. Catal.* 56 (2013) 1634 – 43.

<https://doi.org/10.1007/s11244-013-0098-y>

E. Rocchini, A. Trovarelli, J. Llorca, G. W. Graham, W. H. Weber, M. Maciejewski, A. Baiker, Relationships between Structural/Morphological Modifications and Oxygen Storage–Redox Behavior of Silica-Doped Ceria. *J. Catal.*, 194 (2000) 461–78.

<https://doi.org/10.1006/jcat.2000.2954>

E. Rocchini, M. Vicario, J. Llorca, C. Leitenburg, G. Dolcetti, A. Trovarelli, Reduction and Oxygen Storage Behavior of Noble Metals Supported on Silica-Doped Ceria. *J. Catal.*, 211 (2002) 407–21.

<https://doi.org/10.1006/jcat.2002.3719>

H. S. Roh, K.W. Jun, S. E. Park, Methane-reforming reactions over Ni/Ce-ZrO<sub>2</sub>/θ-Al<sub>2</sub>O<sub>3</sub> catalysts, *Appl. Catal. A*, 251 (2003) 275 – 83.

[https://doi.org/10.1016/S0926-860X\(03\)00359-4](https://doi.org/10.1016/S0926-860X(03)00359-4)

J.R. Rostrup-Nielsen, *Catalysis – Science and Technology*, Vol. 5, eds. J. R. Anderson and M. Boudart (Springer, Berlin, 1984), p.1

B.T. Schadel, M. Duisberg, O. Deutschmann, Steam reforming of methane, ethane, propane, butane, and natural gas over a rhodium-based catalyst. *Catal. Today* 142 (2009) 42 – 51.

<https://doi.org/10.1016/j.cattod.2009.01.008>

F.A. Silva, C.E. Hori, A.M. Silva, L.V. Mattos, J. Múnera, L. Cornaglia, F.B. Noronha, E. Lombardo, Hydrogen production through CO<sub>2</sub> reforming of CH<sub>4</sub> over Pt/CeZrO<sub>2</sub>/Al<sub>2</sub>O<sub>3</sub> catalysts using a Pd–Ag membrane reactor. *Catal. Today* 193 (2012) 64 – 73.

<https://doi.org/10.1016/j.cattod.2012.04.014>

P.P. Silva, R.A.R. Ferreira, F.B. Noronha, Carla E. Hori, Hydrogen production from steam and oxidative steam reforming of liquefied petroleum gas over cerium and strontium doped LaNiO<sub>3</sub> catalysts. *Catal. Today* 289 (2017) 211 – 21.

<https://doi.org/10.1016/j.cattod.2016.10.003>

P.P. Silva, F.A. Silva, H.P. Souza, A.G. Lobo, L.V. Mattos, F.B. Noronha, C.E. Hori, Partial oxidation of methane using Pt/CeZrO<sub>2</sub>/Al<sub>2</sub>O<sub>3</sub> catalysts – effect of preparation methods. *Catal. Today* 101 (2005) 31–7.

<https://doi.org/10.1016/j.cattod.2004.12.008>

J. Silvestre-Albero, F. Rodríguez-Reinoso, A. Sepúlveda-Escribano, Improved Metal-Support Interaction in Pt/CeO<sub>2</sub>–SiO<sub>2</sub> Catalysts after Zinc Addition. *J. Catal.* 210 (2002) 127 – 36.

<https://doi.org/10.1006/jcat.2002.3670>

A. Slagtern, U. Olsbye, R. Blom, I. M. Dahl, H. FjellvSg, In situ XRD characterization of La-Ni-Al-O model catalysts for CO<sub>2</sub> reforming of methane. *Appl. Catal. A*, 145 (1996) 375 – 88.

[https://doi.org/10.1016/0926-860X\(96\)00157-3](https://doi.org/10.1016/0926-860X(96)00157-3)

D.L. Trimm, Catalysts for the control of coking during steam reforming. *Catal Today* 49 (1999) 3 – 10. [https://doi.org/10.1016/S0920-5861\(98\)00401-5](https://doi.org/10.1016/S0920-5861(98)00401-5)

D.L. Trimm, Coke formation and minimization during steam reforming reactions. *Catal. Today* 37 (1997) 233 – 38.

[https://doi.org/10.1016/S0920-5861\(97\)00014-X](https://doi.org/10.1016/S0920-5861(97)00014-X)

A. Trovarelli, Catalytic Properties of Ceria and CeO<sub>2</sub>- Containing Materials, *Catalysis Reviews* 38, 4 (1996) 439 – 520.

<https://doi.org/10.1080/01614949608006464>

A. Trovarelli, M. Boaro, E. Rocchini, C. Leitenburg, G. Dolcetti, Some recent developments in the characterization of ceria-based catalysts. *J. Alloys Compd.* 323–324 (2001) 584–91.

[https://doi.org/10.1016/S0925-8388\(01\)01181-1](https://doi.org/10.1016/S0925-8388(01)01181-1)

H.Z. Wang, D.Y.C. Leung, M.K.H. Leung, M. Ni, A review on hydrogen production using aluminum and aluminum alloys. *Renew. Sust. Energ. Rev.*, 13 (2009) 845–53.

<https://doi.org/10.1016/j.rser.2008.02.009>

S. Wang, G.Q. Lu, Role of CeO<sub>2</sub> in Ni/CeO<sub>2</sub> ± Al<sub>2</sub>O<sub>3</sub> catalysts for carbon dioxide reforming of methane. *Appl. Catal. B*, 19 (1998) 267-77.

[https://doi.org/10.1016/S0926-3373\(98\)00081-2](https://doi.org/10.1016/S0926-3373(98)00081-2)

X. Wang, N. Wang, J. Zhao, L. Wang, Thermodynamic analysis of propane dry and steam reforming for synthesis gas or hydrogen production. *Int. J. Hydrogen Energy* 35 (2010) 128000 – 7.

<https://doi.org/10.1016/j.ijhydene.2010.08.132>

Y.H.T. Yap, Sudarno, U. Rashid, Z. Zainal, CeO<sub>2</sub>-SiO<sub>2</sub> supported nickel catalysts for dry reforming of methane toward syngas production. *App. Catal. A*, 468 (2013) 359– 69.

<https://doi.org/10.1016/j.apcata.2013.09.020>

D. Zanchet, J.B. Santos, S. Damyanova, J.M.R. Gallo, J.M.C. Bueno, Towards Understanding Metal-Catalyzed Ethanol Reforming. *ACS Catal.* 5, 6 (2015) 3841 – 63.

<https://doi.org/10.1021/cs5020755>

L. Zhang, X. Wang, B. Tan, U. S. Ozkan, Effect of preparation method on structural characteristics and propane steam reforming performance of Ni-Al<sub>2</sub>O<sub>3</sub> catalysts. *J. Mol. Catal. A*, 297 (2009) 26 – 34.

<https://doi.org/10.1016/j.molcata.2008.09.011>

X. Zhao, H. Li, J. Zhang, L. Shi, D. Zhang, Design and synthesis of NiCe@m-SiO<sub>2</sub> yolk shell framework catalysts with improved coke- and sintering-resistance in dry reforming of methane. *Int. J. Hydrogen Energy*, 41 (2016) 2447-56.

<https://doi.org/10.1016/j.ijhydene.2015.10.111>

X. Zhao, Y. Xue, Z. Lu, Y. Huang, C. Guo, C. Yan, Encapsulating Ni/CeO<sub>2</sub>-ZrO<sub>2</sub> with SiO<sub>2</sub> layer to improve its catalytic activity for steam reforming of toluene. *Catal. Commun.*, 101 (2017) 138–41.

<https://doi.org/10.1016/j.catcom.2017.08.013>

L. Zhou, L. Li, N. Wei, J. Li, J. Basset, Effect of NiAl<sub>2</sub>O<sub>4</sub> Formation on Ni/Al<sub>2</sub>O<sub>3</sub> Stability during Dry Reforming of Methane. *ChemCatChem* 7 (2015) 2508 – 16.

<https://doi.org/10.1002/cctc.201500379>

M.G. Zimicz, F.D. Prado, D.G. Lamas, S.A. Larrondo, In-situ XANES and XPD studies of NiO/Ce<sub>0.9</sub>Zr<sub>0.1</sub>O<sub>2</sub> IT-SOFCs anode nanomaterial as catalyst in the CPOM reaction. *Appl. Catal. A*, 542 (2017) 296–305.

<https://doi.org/10.1016/j.apcata.2017.05.040>